LANGMUIR

Interfaces: Adsorption, Reactions, Films, Forces, Measurement Techniques, Charge Transfer, Electrochemistry, Electrocatalysis, Energy Production and Storage

Assembly of T-Shaped Amphiphilic Thiazoles on the Air-Water Interface: Impact of Polar Chromophore-Moieties, as well as Dipolarity and #-Extension of the Chromophore on the Supramolecular Structure

Maximilian Lutz Hupfer, Martin Kaufmann, Julia Preiß, Dieter Weiss, Rainer Beckert, Benjamin Dietzek, and Martin Presselt

Langmuir, **Just Accepted Manuscript** • DOI: 10.1021/acs.langmuir.8b04063 • Publication Date (Web): 28 Jan 2019

Assembly of T-Shaped Amphiphilic Thiazoles on the Air-Water Interface: Impact of Polar Chromophore-Moieties, as well as Dipolarity and π-Extension of the Chromophore on the Supramolecular Structure

Maximilian L. Hupfer[1,3], Martin Kaufmann[1,2], Julia Preiß[1,3], Dieter Weiß[2], Rainer Beckert[2], Benjamin Dietzek[1,3], Martin Presselt[1,3,4,5*]

[1] Institute of Physical Chemistry, Friedrich Schiller University Jena, Helmholtzweg 4, 07743 Jena, Germany, E-mail: martin.presselt@leibniz-ipht.de, Phone: +49 3641 206418

[2] Institute of Organic and Macromolecular Chemistry, Friedrich Schiller University Jena, Humboldstraße 10, 07743 Jena, Germany

[3] Leibniz Institute of Photonic Technology (IPHT), Albert-Einstein-Str. 9, 07745 Jena, Germany

[4] Center for Energy and Environmental Chemistry Jena (CEEC Jena), Friedrich Schiller University Jena, Philosophenweg 7a, 07743 Jena, Germany

[5] sciclus GmbH & Co. KG, Moritz-von-Rohr-Str. 1a, 07745 Jena, Germany

*Corresponding author: martin.presselt@leibniz-ipht.de

KEYWORDS
Langmuir-Blodgett; Langmuir isotherm; non-covalent interactions; organic electronics; aggregate; in situ fluorescence

ABSTRACT

The supramolecular structure essentially determines the properties of organic thin films. In this work we systematically investigate the influence of the chromophore on the supramolecular structure formation at air-water interfaces by means of the Langmuir-Blodgett (LB) technique. Therefore, we focus on the recently introduced class of double-anchor T-shaped amphiphilic dyes, namely 4-hydroxy-thiazole chromophores that are centrally equipped with an amphiphilicity-inducing hexanoic acid. The thiazoles contain hydrophilic subphase-anchor groups in the 2-position (4-N,N-dimethylaminophenyl (**Am**), 2-pyridyl (**Py**), and 4-nitrophenyl (**Ni**)), while the chromophores are systematically extended in the 5-position with various substituents. The combination of Langmuir technique with online fluorescence measurements revealed that the ππ-interactions that are pronounced in case of 4-methoxybiphenyl derivatives yield the most distinct supramolecular structures: While in case of **Py**- and **Ni**-derivatives ordered J-type supramolecular structures in microdomains are formed, the **Am**-derivative forms ordered supramolecular structures that are more homogeneous, which are, however, not stabilized by J-type dipolar interactions. Because of the synergetic ππ- and dipolar stabilizations the **Ni**-derivative bearing the 4-methoxybiphenyl unit forms exceptionally stable quasi-two-dimensional Langmuir monolayers reaching very high surface pressures beyond 60 mN/m without any sign of disturbance of the Langmuir monolayer.

INTRODUCTION

Organic (opto)electronic devices like solar cells (OSCs)[1], light emitting diodes (OLEDs)[2], and field effect transistors (OFETs)[3] are steadily gaining importance. The active layer and device properties, especially spectral[4, 5, 6, 7, 8] and radiative[9, 10] characteristics, external quantum efficiency[11, 12, 13, 14, 15], open circuit voltage[16], conductivity[17, 18, 19, 20], excited state dynamics[21, 22, 23], and electrochemical potentials[4, 24, 25] are tuned by engineering the molecular characteristics and the supramolecular structure. To control supramolecular structures several techniques, like antiparallel supramolecular arrangement of dipolar donor-acceptor dyes[26, 27], co-self-organization [28], layer-by-layer deposition (LbL) [29, 30], and (self)assembly at heterointerfaces, have been developed. Another valuable technique that allows for advanced control of the supramolecular structure formation at liquid-gas interfaces is the Langmuir-Blodgett (LB) technique,[31, 32, 33, 34] which enables supramolecular tuning of optical and optoelectronic properties of functional amphiphiles.[4, 35, 36]

The supramolecular geometries and their optoelectronic properties inherently depend on the molecular parameters[37, 38, 39, 40], such as the chromophore, chemical nature, number and position of polar and non-polar moieties in the amphiphile. It was shown that even the lengths and the type of spacers[41] between polar and non-polar as well as the specific chemical nature of the polar moieties[41, 42, 43] heavily influence the geometries of supramolecular structures formed at the air-water interface. Recently, novel T-shaped amphiphilic dyes have been presented in which the amphiphilicity-introducing hexanoic acid is linked centrally to rather hydrophobic chromophores.[41, 44, 45, 46] The flexibility of the hexanoic acid[41], but also the tunable polarity of the chromophore, particularly introduction of second hydrophilic subphase anchor groups and introduction of dipolarity,[45] make this class of amphiphiles highly versatile and enables formation of different supramolecular structure at the air-water interface.[41, 44, 45]

Basically just two different types of chromophores from this type of T-shaped amphiphiles have been reported in the literature so far.[45] Here, we attempt to systematically study the influence of chemical variations of the chromophore (see **Scheme 1**) on the formation of supramolecular structures on air-water interfaces and the resulting optical properties. The large number of supramolecular structures that can form from the high number of investigated derivatives at varied Langmuir parameters are characterized *via* analysis of the Π(A) isotherm and *in situ* fluorescence measurements[47]. UV-vis spectroscopy has been demonstrated to enable determination of interactions of the dye with the subphase[47] and thermodynamics in amphiphile mixtures[48], or changes of the supramolecular geometry[43].

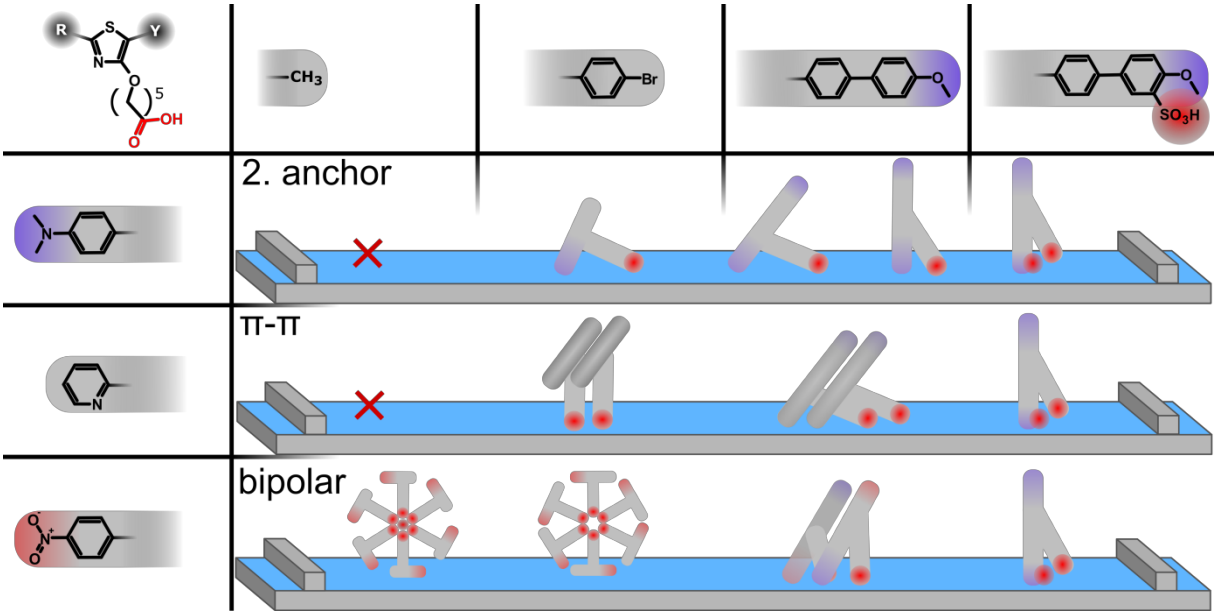

Scheme 1: Central attachment of a hydrophilic head group to a thiazole chromophore, which is systematically varied on the 2- and 5-position, *via* an alkylic linker yields a "T-shaped" amphiphile with various intra- and intermolecular interactions in a Langmuir monolayer

The T-shaped amphiphiles derived from 4-hydroxy-thiazoles are predestined for *in situ* fluorescence characterization as they often feature high fluorescence quantum yields (up to 95% in water[49]). Because of the corresponding slow non-radiative excited state decay, 4-hydroxy-thiazoles have been tested for application in dye-sensitized solar cells (DSSCs)[50], as blue emitters in polymer backbones[51, 52] and as oligomers in organic field effect transistors[53]. In this work the thiazole chromophore is varied by introducing three different hydrophilic subphase anchors in the 2-position of the thiazole, namely 4-N,N-dimethylaminophenyl (**Am**), 2-pyridyl (**Py**), and 4-nitrophenyl (**Ni**).[54, 55] Furthermore, the chromophore gets systematically π-extended in the 5-position for each of the anchor functions by substituting the methyl group (**Me**) by a 4-bromophenyl (**Br**), and 4-methoxybiphenyl (**Bi**). Finally, the chromophores are additionally equipped with a third hydrophilic anchor, a 4-methoxyphenyl-3-sulfonylphenyl (**BiSulf**) moiety. After presenting the synthesis these systematically varied amphiphilic T-shaped thiazoles, their optical properties in solution and at an air-water interface are determined and compared with mean molecular areas derived from Langmuir experiments to understand the film formation and to derive schemes of supramolecular structures formed at the air-water interface.

RESULTS AND DISCUSSION

To investigate a broad range of the effects of the chromophore, three different core units of the thiazoles were selected as target structures. A *N*,*N*-dimethylaminophenyl-derivative was selected to represent electron rich substituents, a nitrophenyl-derivative as electron deficient substituent and a 2-pyridyl-derivative as a "neutral", heterocyclic derivative. Based on the three core units, the electron rich dimethylphenyl thiazole, the electron deficient nitrophenyl thiazole and the "neutral", hetrocyclic pyridyl thiazole, three successively expansions (methyl group, bromphenyl group, methoxybiphenyl group, sulfonation) of the π-system are targeted. The synthetic route is depicted in **Figure 1**.

Starting from the nitriles **1**, the 5-methyl thiazoles **3** are accessible by the *Erlenmeyer Route*, in which the nitrile is condensed with thiolactic acid **2**, as shown in Figure 1. According to the method by Calderon[56] the pyridyl derivative and the nitro derivative **Ni 3** were obtained in 76-81% yields. However, the amino thiazole couldn't be isolated because of degradation while the work up procedure. The alkylation with ethyl 6-bromo-hexanoate not only increases the solubility of the dye but build up the precursor for the amphiphilic anchor group. It was performed by standard procedure, which is published for 4-hydroxy-thiazoles[50, 57, 58]. For the second π-expansion step, the thiazoles core units has to be synthesized with the well-established *Hantzsch thiazole synthesis*[59, 60, 61]. Starting from the thioamides **(Am/Py/Ni) 5** the condensation with **6** leads to the 5-Bromophenyl-4-hydroxy thiazoles **7** which were obtained in very good yields from 60 to 87%. The following alkylation iv was carried out under the same conditions as in reaction step ii and alkoxy thiazoles **8** were obtained in 72-83% yields. A further expansion of the chromophore is possible by cross coupling of the 5-(4-bromophenyl)-substituent. Several different cross coupling reactions, like *Buchwald-Hartwig Aminations*[58, 62], *Sonogashira Cross-Coupling*[63] or *Stille Cross Couplings* are already described for 5-Bromophenyl thiazoles. Still no *Suzuki reactions* on these dyes are known up to date. However, Arcardi[64] *et al*. performed various *Suzuki cross couplings* on 4-triflyl thiazoles, which are structural comparable to our target molecules. With a slight variation of this method (changing the catalyst from $Pd(PPh_3)_4$ to $Pd(PPh_3)_{PyBi}I_2$) the 5-(4-methoxybiphenyl)-thiazoles **9** were obtained in moderate 31-56% yields. With the successful syntheses of **4, 8** and **9** the ester group of the hexanoate sidechain needs to be saponificated to yield the amphiphilic anchor group. Recently the deprotection of such alkyl esters of 4-alkyoxy thiazoles was published, using a anhydrous ethanolic potassium hydroxide solution[41, 42]. Using this procedure, the aminothiazoles **AmBr** and **AmBi**, the pyridylthiazoles **PyMe**, **PyBr** and **PyBi** and the nitrothiazoles **NiMe**, **NiBr**, **NiBi** were isolated in very good yield from 87-95%. Finally the 5-(4-methoxybiphenyl)-thiazoles **AmBi**, **PyBi** and **NiBi** were sulfonated by the method of Habenicht[43]. All target molecules except the sulfonated **AmBiSulf**,

PyBiSulf and **NiBiSulf** are good soluble in chloroform or dichloromethane, which are suitable solvents for the Langmuir technique. The sulfonic acid group increases the hydrophilicity thus the best solubility of these was observed in methanol. However a mixture of chloroform and methanol can be used to achieve the necessary minimum solubility for the Langmuir technique.

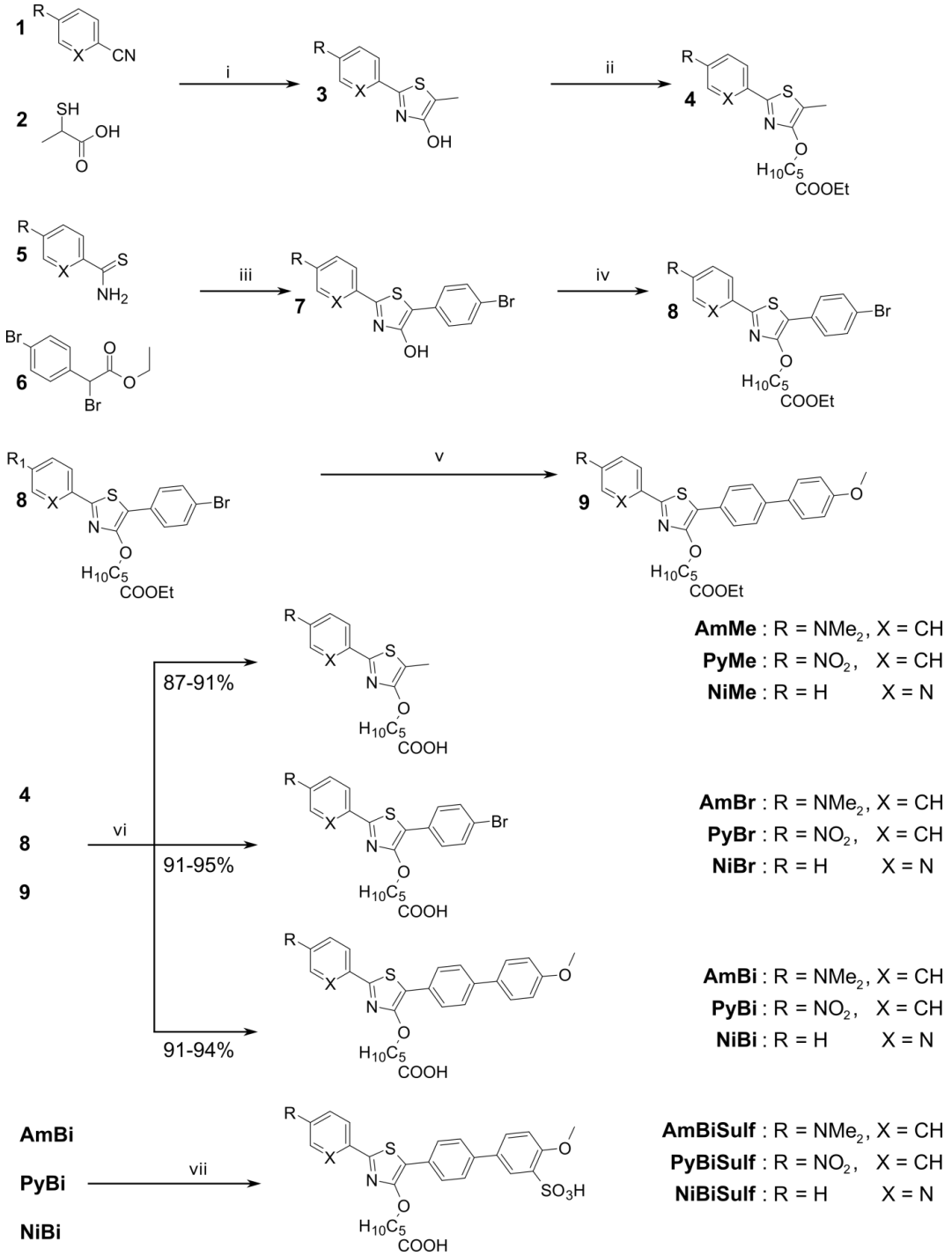

Figure 1: Synthetic route to the target compounds; i) pyridin, ΔT, 0-81%; ii) $BrC_5H_{10}CO_2Et$, $K_{PyBi}O_3$, acetone , ΔT, 64-73%; iii) NaOAc, EtOH, ΔT, 60-87%; iv) $BrC_5H_{10}CO_2Et$, $K_{PyBi}O_3$, acetone , ΔT, 72-83%; v) *p*-OMePh-B(OH)$_2$, $K_{PyBi}O_3$, $Pd(PPh_3)_{PyBi}I_2$, thf, ΔT, 31-56%; vi) KOH, EtOH (abs.) , 50°C; vii) AcOH, H_2SO_4, RT – 50°C, 23-39%.

UV-vis Absorption and Fluorescence Spectroscopy

The influence of the above introduced modifications to the thiazole chromophores are characterized by means of UV-vis absorption and fluorescence spectroscopy in solution. The variation in solvent polarity yields reference spectra for the thiazoles in different supramolecular environments studied in the subsequent Langmuir sections.

Table 1. Extinction coefficients ($\varepsilon(\lambda_{max})$) (determined *via* linear regression for concentrations ranging from $c = 10^{-4}$ M to 10^{-7} M, see supporting information Figure Si 64-71), spectral positions of absorption and emission maxima ($c < 10^{-6}$M) of 2-(4-N,N-dimethylaminophenyl/2-pyridyl/4-nitrophenyl)-4-hydroxy-5-Y-1,3 thiazoles with different functionalization

		TD-DFT	**Toluene**			**$CHCl_3$**			**CH_3OH**		
		S_0 -> S_1	***dielectric constant: 2.4***			***dielectric constant: 4.8***			***dielectric constant: 33***		
R	Y	vac [nm]	ε [$M^{-1}cm^{-1}$]	abs [nm]	em [nm]	ε [$M^{-1}cm^{-1}$]	abs [nm]	em [nm]	ε [$M^{-1}cm^{-1}$]]	abs [nm]	em [nm]
Am	**Me**	355									
	Br	403	40.724	396	483	39.204	394	485	43.611	391	485
	Bi	415	51.712	400	494	48.833	400	497	75.764	396	496
	BiSulf	419			458		400	469		397	496
Py	**Me**	353	12.512	347	420	9.127	345	420	11.145	342	422
	Br	400	12.274	376	452	22.696	375	454	27.882	375	455
	Bi	422	43.656	393	479	36.612	392	482	28.652	386	492
	BiSulf	408						478		386	484
Ni	**Me**	429	18.524	391	500	27.348	393	588	23.944	383	450
	Br	476	19.525	419	525	30.201	423	615	24.965	411	450
	Bi	519	26.037	436	562	36.091	439	689	44.795	426	484
	BiSulf	487		432	546		430	669		425	485

4-N,N-Dimethylaminophenyl Derivatives

The extinction coefficient ($\varepsilon(\lambda)$) spectra of **Am** (**Figure 2**) show a pronounced single absorption peak (*cf.* quantum chemical results shown in the Supporting Information (SI) Figure SI 37) with an increase of ε and a slightly red-shift upon extension of the π-electron system[63] from **AmBr** to **AmBi** (**Figure 2**). In **AmBi**, the CH_3O-group adds a weak electron donating (D) character[65] to the chromophore and complements its DπD character, what causes an additional red-shift in the absorption. Introduction

of an additional SO_3Hgroup (**AmBiSulf**) significantly decreases the solubility in non- and slightly polar solvents and does not notably shift the absorption maximum as compared to **AmBi**. In agreement with recent reports on thiazole chromophores, their absorption spectra negligibly blue-shift upon increased solvent polarity.[44]

However, the extension of the π-electron system causes a red-shifted emission for the different Y functionalizations from **AmBr** to **AmBiSulf**. As an exception, the emission spectrum of **AmBiSulf** shows a slightly blue-shifted emission in non- and aprotic polar solvents (toluene, $CHCl_3$), as compared to **AmBi**, what might be attributed to the presence of ground state aggregates and a stabilization of excited states. Additionally, dipolar aggregation could cause a protonation of the $(CH_3)_2N$-group by the SO_3H moiety.

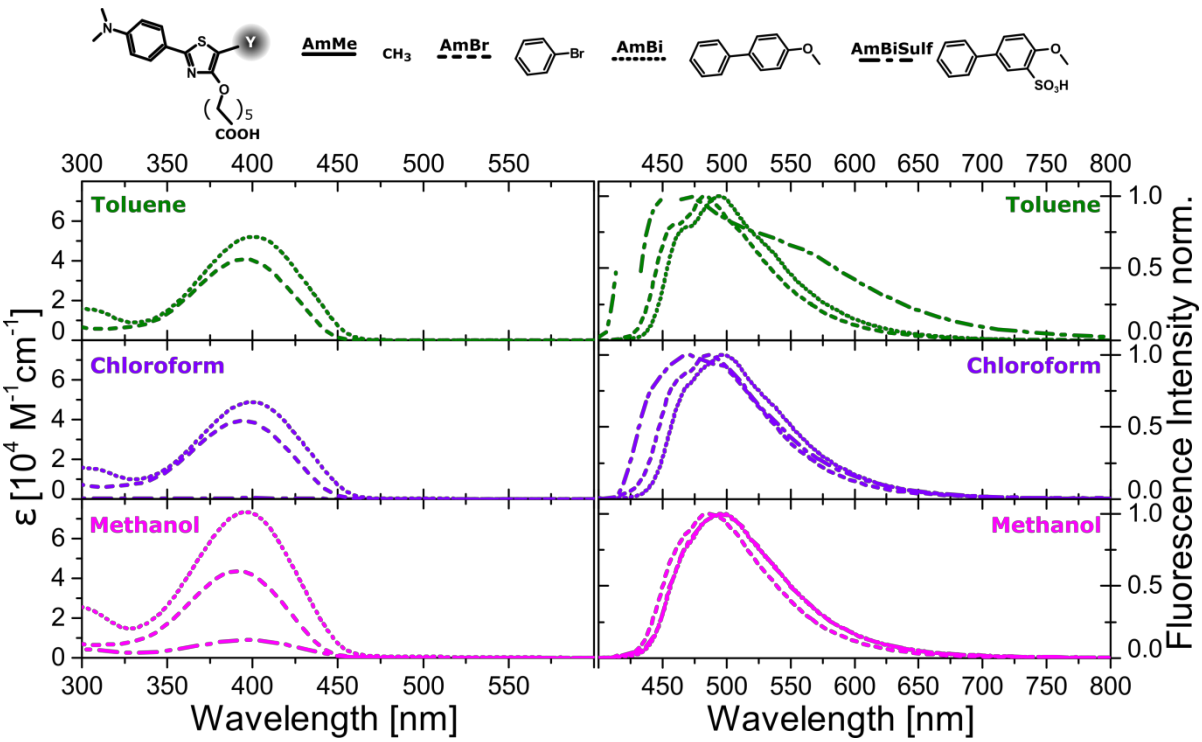

Figure 2: Extinction coefficient (ε) (left) and normalized emission (right) of the 2-(4-N,N-dimethyl-aminophenyl)-4-hydroxy-5-Y-1,3 thiazole core (λ_{exc}=405 nm) and the methyl (**AmMe**) (solid), phenyl-4-bromo (**AmBr**) (dotted), phenyl-4-methoxyphenyl (**AmBi**) (dashed) and 3-phenyl-4-methoxyphenyl-3-sulfonylphenyl (**AmBiSulf**) (dotted dashed) functionalization in toluene (dark green, upper row), $CHCl_3$ (violet, middle row), CH_3OH (pink, lower row) ($c < 10^{-6}$M)

2-Pyridyl Derivatives

The extinction coefficient and emission spectra of the **Py**-derivatives significantly red-shift upon extension of the π-system, as shown in **Figure 3**. Hence, while in case of **Am** the absorption and

emission properties were largely determined by the electron-pushing amine moiety, the pyridine moiety in **Py** enables enlarging the chromophoric unit upon attaching phenylene groups.

However, all spectra of the **Py**-derivatives are blue-shifted as compared to their **Am**-counterparts (compare **Figure 2** with **Figure 3**; see **Table 1**), what is in agreement with reports on similar chromophores.[63] This difference in the spectral position increases with shortening of the π-system, *i.e.*, as most pronounced for the (**Am**/**Py**)**Me** derivatives. As mentioned for **AmBiSulf** above, an introduction of a SO_3H-group at the 4-methoxybiphenyl moiety (**PyBiSulf**) significantly decreases solubility in non-polar solvents and again, the emission shifts slightly blue due to aggregation in toluene and $CHCl_3$.

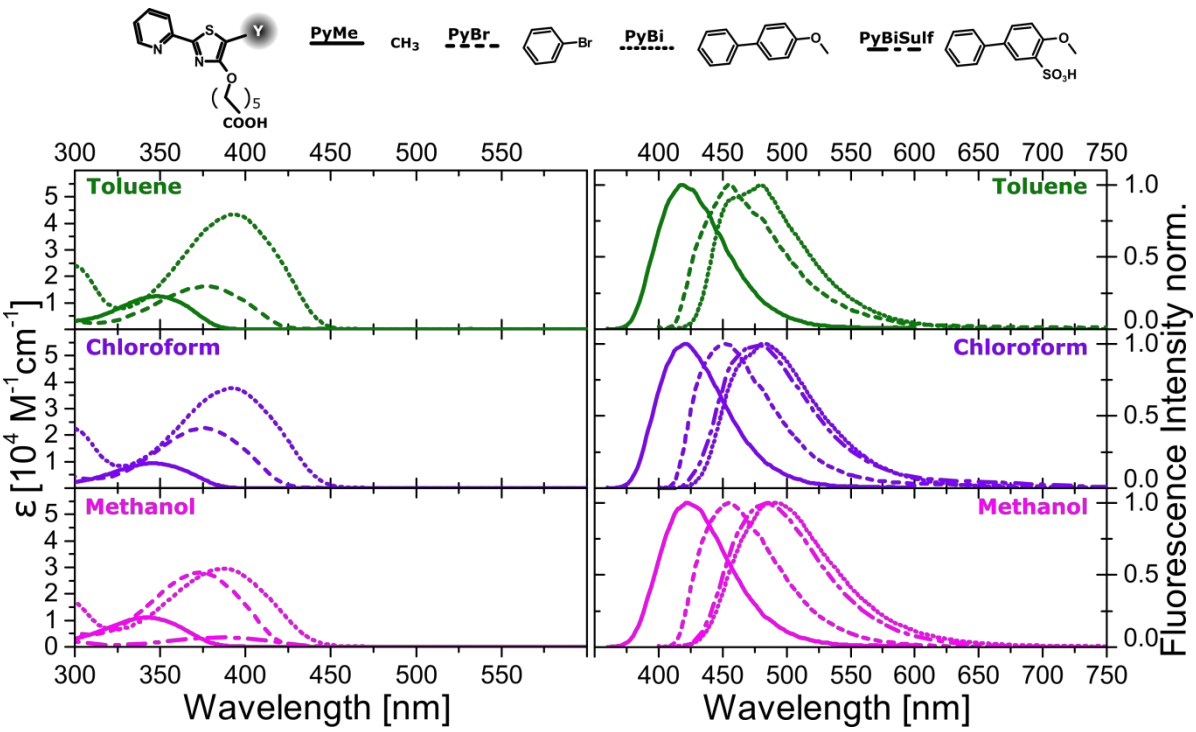

Figure 3: Extinction coefficient (ε) (left) and normalized emission (right) of the 2-(2-pyridyl)-4-hydroxy-5-Y-1,3 thiazole core (405 nm) methyl (**PyMe**) (solid), phenyl-4-bromo (**PyBr**) (dotted), phenyl-4-methoxyphenyl (**PyBi**) (dashed) and 3-phenyl-4-methoxyphenyl-3-sulfonylphenyl (**PyBiSulf**) (dotted dashed) functionalization in toluene (dark green, upper row), $CHCl_3$ (violet, middle row), CH_3OH (pink, lower row) ($c < 10^{-6}$M)

4-Nitrophenyl Derivatives

Similar to the **Py**-thiazoles before, the **Ni**-derivatives show red-shifted absorption (**Figure 4**) upon extension of the π-system through the different Y-functionalizations. In contrast to **Am** and **Py**, the **Ni**-derivatives show a pronounced solvent-dependence of their fluorescence spectra, as shown in **Figure 4**. While the fluorescence spectra of **Ni** dissolved in methanol are similar to those of **Am** and **Py** (λ_{max} = 450-500 nm, **Am** and **Py** in all solvents), they significantly red-shift to λ_{max} = 500-575 nm in case the **Ni** derivatives are dissolved in toluene. A further red-shift to λ_{max} = 575-700 nm is observed if

the solvent is $CHCl_3$. In case of **NiBi** an additional peak between 450-500 nm is present in the $CHCl_3$ fluorescence spectrum. This peak, which features vibrational progression similar to the spectra of **NiBi** and **NiBiSulf** dissolved in CH_3OH, actually dominates the fluorescence spectra of the polar **NiBiSulf** derivatives when dissolved in $CHCl_3$.

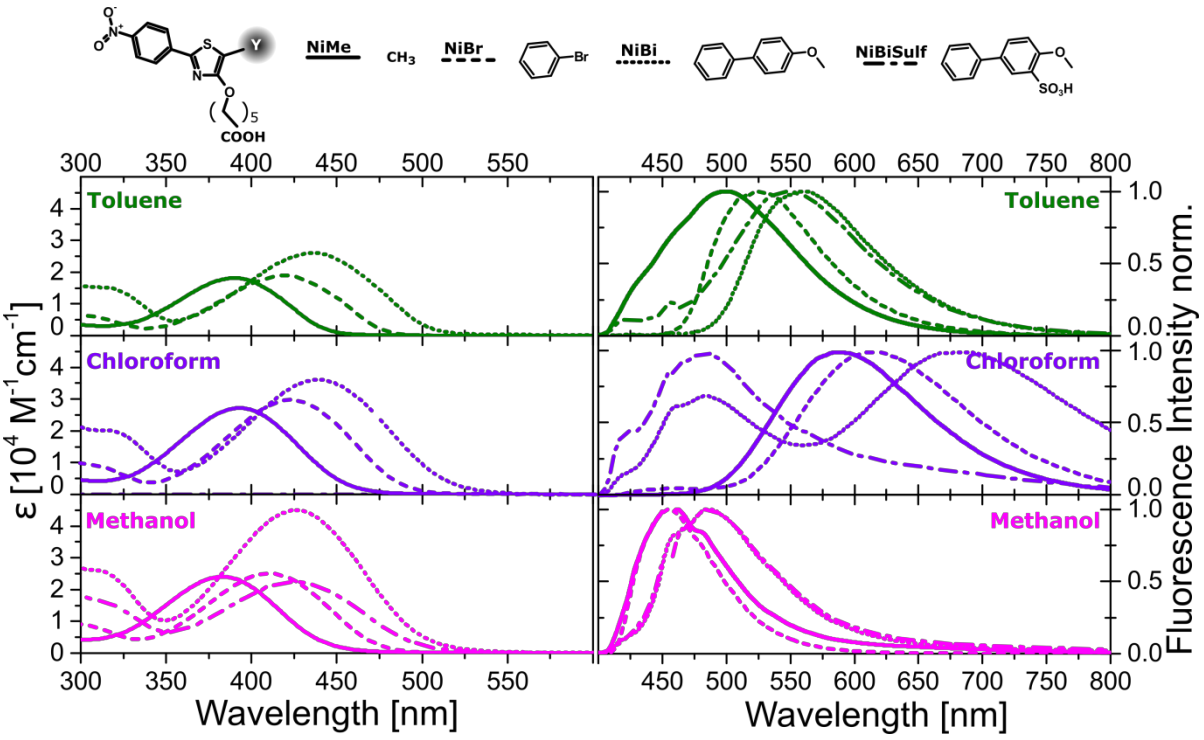

Figure 4: Extinction coefficient (ε) (left) and normalized emission (right) of the 2-(4-nitrophenyl)-4-hydroxy-5-Y-1,3 thiazole core (λ_{exc}=405 nm) methyl (**NiMe**) (solid), phenyl-4-bromo (**NiBr**) (dotted), phenyl-4-methoxyphenyl (**NiBi**) (dashed) and 3-phenyl-4-methoxyphenyl-3-sulfonylphenyl (**NiBiSulf**) (dotted dashed) functionalization in toluene (dark green, upper row), $CHCl_3$ (violet, middle row), CH_3OH (pink, lower row) ($c < 10^{-6}$M)

To elucidate the origin of the dual emission of **NiBi** when dissolved in $CHCl_3$ (**Figure 4**) dilution studies have been performed to reveal the possible presence of molecular aggregates that might cause either of the fluorescence peaks. Variation of the concentration of **NiBi** in both solvents changes systematically the ratio between the dual emission peaks, as shown in **Figure 5**a and b. Because the fluorescence peak between 450 and 500 nm rises upon increasing concentration (**Figure 5**b), it is assigned to molecular aggregate fluorescence, while the 690 nm-emission must originate from the monomer. The corresponding aggregate absorption, which is virtually invisible in the absorption spectra in **Figure 4**, peaks at 378 nm, as revealed by photoluminescence excitation spectroscopy in **Figure 5**c. Because of the blue-shift and the dipolar chromophore character of the **Ni**-derivatives, the aggregates are presumed to be of H-type. Interestingly, when dissolved in methanol the dimer emission dominates the fluorescence spectrum, while the monomer emission cannot be detected.

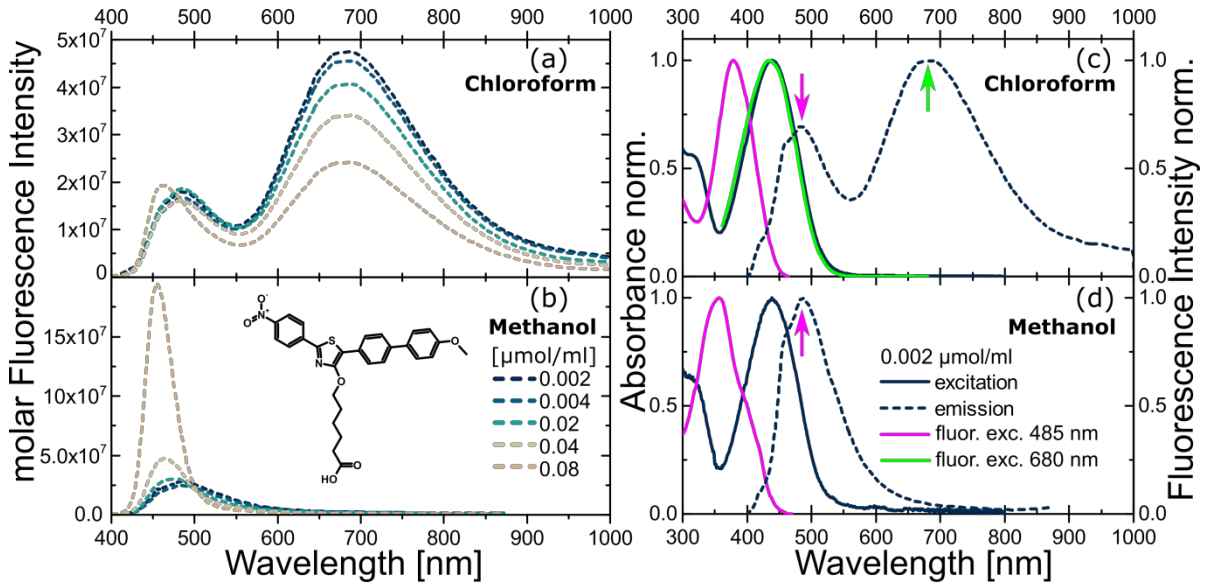

Figure 5: Molar and self-absorption corrected emission spectra of **NiBi** in $CHCl_3$ (a) and CH_3OH (b) (*cf.* 0.002 µmol/ml Figure 4) at five different concentrations. Excitation (dark blue, solid), emission (dark blue, dashed, λ_{ex}=405 nm) and fluorescence excitation spectra at λ_{em}=485 nm (green) and λ_{em}=700 nm (pink) of **NiBi** in $CHCl_3$ (c) and CH_3OH (d) (0.002µmol/ml)

Finally, **Am** and **Py** show similar monomeric absorption and emission features and the same dependencies on molecular substitutions, namely the **Me**, **Br**, **Bi**, and **BiSulf** substituents causing red-shifts of the absorption and emission spectra with successive π-system extension (**Bi** always yielding the largest red-shift). These results are in good agreement with the literature.[41, 42, 43, 63] While the **Am** and **Py** derivatives easily dissolve in the broad range of differently polar solvents (except their **BiSulf** derivatives), the **Ni** derivatives show fluorescence peaks assigned to aggregates, even in the dilute solutions. Because of their spectral shifts as compared to the monomers we deduce dipolar aggregation in case of the **Ni** derivatives, which is expected to impact supramolecular structure formation at the air-water interface[45] as discussed in the following.

Π(A)-Isotherms

In general, surface pressure (Π) *vs.* mean molecular area (A) isotherms indicate the formation of two-dimensional monolayers featuring possibly different supramolecular structures, transitions between them, and their breakdown.[41, 66] The supramolecular structures of these monomolecular Langmuir films are characterized by the molecular packing density or molecular orientations, which are deduced from the extrapolated minimum molecular area (A_0: derived from steep sections (*cf.* compressibility modulus shown in Figure SI 64) of the Π(A)-isotherm). To assign distinct supramolecular structures to Langmuir monolayers the experimentally determined A_0-areas are compared to theoretically derived A_0-areas of molecular conformations assumed to be possible at

the air-water interface.[41] The molecular orientations in the individual condensed phases are then identified by the best fit between theoretical and experimental A_0-areas.

As shown in **Figure 6**, no Π(A)-isotherms rising at physically meaningful areas were detected for **Me**-derivatives (Y=CH_3), which turn out to be water-soluble and not sufficiently amphiphilic for the use in the Langmuir technique. The isotherms further reveal that the largest A_0-areas observed do not exceed 50 Å². This small area shows that condensed phases are not formed from flat aligned amphiphiles (parallel to the water surface, thus necessitating areas significantly larger than the measured A_0-areas) but instead the chromophores must be partially dissolved in the aqueous subphase and vertically aligned or tilted when the Langmuir monolayers are formed. The maximum A_0-areas are obtained for the largest non-polar Y-substituents of type **Bi** for any of the thiazoles, *i.e.* **AmBi**, **PyBi**, **NiBi**.

4-N,N-Dimethylaminophenyl Derivatives

The Π(A)-isotherm of **AmBr** in **Figure 6** (left) shows a stable and compressible monolayer between 44 and 35 Å² (A_0 = 44 Å², **Table 2**). A similar A_0-area $A_{0,theo}$ = 43 Å², shown in **Figure 6** (**AmBr**), is also obtained when multiplying the molecular length between the COOH, which works as the anchor group to the water subphase, and **Am** (the $(CH_3)_2N$-group, 16.4 Å²) with the sulfur van der Waals diameter (2.6 Å). As we have shown previously[44], in this supramolecular orientation the $(CH_3)_2N$ substituent works as a second anchor[67] because of its basicity (N,N-dimethylaniline, pK_a = 5.1[68]; *cf.* heptaonic acid, pK_a = 4.4[69]). Therefore, we conclude that the chromophore is slightly vertically tilted on the water surface and straightens up in the first phase of the stable and compressible monolayer, thus causing a reduction of the distance between the two anchors. Further compressions yield a transition phase of high compressibility, without a second rise of Π. Therefore, we conclude that the collapse point (Π_C) of the monolayer **AmBr** is reached at a surface pressure of Π_C > 8.5 mN/m.

Extending Y to the still rather non-polar 4-methoxybiphenyl moiety (**AmBi**) basically yields just a small shift of +6 Å² (even if now containing a sterically demanding twisted biphenyl moiety) of the isotherm (**AmBi** : A_0 = 50 Å²), and an additional phase (A_{0*} = 15 Å²) is observed, as shown in **Figure 6**. Because this A_{0*}-area is very small, it might be assigned to upright aligned molecules with both anchors dissolved in the subphase, as shown in **Figure 6** (**AmBi***), or to formation of three-dimensional aggregates. Further modification of Y by attaching a SO_3H-group (**AmBiSulf**) significantly shifts the isotherm's onset to smaller mean molecular areas. In accordance to the interpretation of the small A_{0*}-area of **AmBi***, the resulting small A_0–area (14 Å²) of **AmBiSulf** is assigned to partially dissolved or three-dimensionally aggregated chromophores. However, because the SO_3H-group is

more hydrophilic than the $(CH_3)_2N$-group (*cf.* *p*-toluenesulfonic acid[70], $pK_a = -2.8$[71]) the former is expected to function as second anchor instead of the latter.

Table 2. Extrapolated minimum molecular area (A_0) derived from Π(A) isotherm of different 4-hydroxy-5-1,3 thiazoles

Y	**Am**		**Py**		**Ni**	
	A_0 ($A_{0,*}$)		A_0 ($A_{0,*}$)		A_0 ($A_{0,*}$)	
	exp	theo	exp	theo	exp	theo
	[Å^2]	[Å^2]	[Å^2]	[Å^2]	[Å^2]	[Å^2]
Me	/	/	1	/	4 (4)	/
Br	44	43	18	18	25 (15)	/
Bi	50 (15)	51 (18)	47	48	33	/
BiSulf	16	18	14	18	21	/

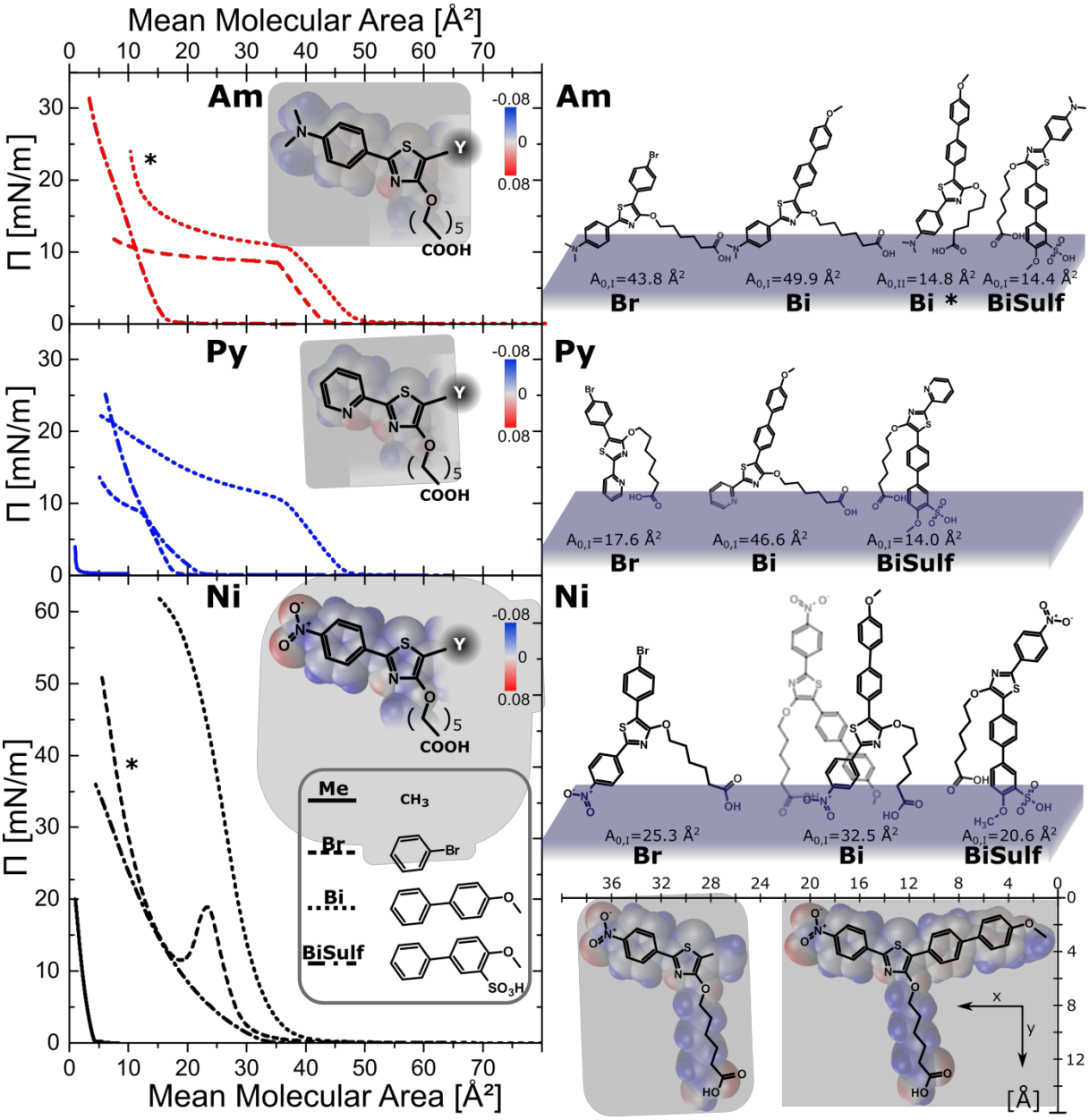

Figure 6: (left) Averaged mean Π(A) isotherms of (**Am**) 2-4-N,N-dimethylaminophenyl-; (**Py**) 2-2-pyridyl; (**Ni**) 2-4-nitrophenyl-4-hydroxy-5-Y-1,3 thiazoles and the methyl (**Me**, solid), phenyl-4-bromo (**Br**, dotted), phenyl-4-methoxyphenyl (**Bi**, dashed) and 3-phenyl-4-methoxyphenyl-3-sulfonylphenyl (**BiSulf**, dotted dashed) functionalization. (right) Molecular orientations of the different 4-hydroxy thiazoles in the Langmuir film derived from the extrapolated minimum molecular area (A_0) of the Π(A) isotherm. Exemplarily, the representative molecular dimension of **NiMe** and **NiBi** are given. Lewis structures are plotted on top of images of the electrostatic potential (ϕ) distribution at the van der Waals surface.

2-Pyridyl Derivatives

With the change to a 2-(2-pyridyl) substitution at the thiazole the molecular amphiphilicity is significantly altered. The Π(A) isotherm of **PyBr** starts rising at 22 Å² (A_0 = 17.6 Å²; see **Figure 6**). Such a small A_0 area is obtained when multiplying the molecular y-lengths of **PyBr** (from the sulfur to the oxygen of the 4-hydroxy-5-Y-1,3 thiazoles y=6.4 Å , see **Figure 6**) with the vdW diameter of sulfur. This

A_0 area corresponds to a previously reported one for the same chromophore without the bromine.[41] Therefore, we expect a supramolecular structure where the chromophore is tilted with the Py-group dissolved in the water subphase due to its polarity and acidity (pyridine, $pK_a = 5.14$[72]). Subsequently, the isotherm-section being characteristic for **PyBr** is followed by a second rise of the Π(A) isotherm after passing a pronounced bend.

Extending Y to a still rather non-polar 4-methoxybiphenyl moiety increases the A_0 areas by 20 Å² (**PyBi** : A_0 = 46.6 Å²) and again no second condensed phase is observed till the minimum trough area is reached. We assign the large A_0 area to a tilted molecule with both anchors dissolved in the subphase, as shown **Figure 6** (**PyBi**). Similar to **AmBiSulf**, attaching of SO_3H (**PyBiSulf**) significantly shifts the A_0 area to smaller values and yields a liquid condensed phase. In accordance to the interpretation of the small A_{0*} area of **PyBi***, the resulting very small A_0 area (14 Å²) of **PyBiSulf** is assigned to upright aligned and partially dissolved or three-dimensionally aggregated chromophores (**Figure 6**, **PyBiSulf**).

4-Nitrophenyl Derivatives

Introduction of nitrophenyl instead of aminophenyl or pyridine replaces the second strong anchor[73, 74] by a less polar moiety. The Π(A) isotherm for the molecule **NiBr** with a Y = bromophenyl functionalization shows a highly compressible liquid phase with increasing Π at A < 40 Å² that transforms to a condensed phase of lower compressibility at higher surface pressures and decreased areas (A_0 = 25 Å²), *cf.* **AmBr** and **PyBr** above. A peak in the isotherm at A = 23 Å² (18 mN/m) indicates a collapse or strong reorganization of this first stable and compressible monolayer. At further compressions the surface pressure steeply rises till Π > 50 mN/m, which indicates the formation of a second phase of a condensed **NiBr** monolayer with rather low compressibility[42] (compressibility modulus reaching 140 mN/m, as shown in Figure SI 64). The latter is, similar to **Am-** and **PyBr**, characterized by A_{0*} = 15 Å².

Extension of Y to a 4-methoxybiphenyl moiety (**NiBi**) also adds a third somewhat dipolar group (OCH_3) to the amphiphile, as shown by the electrostatic potential distribution at the van der Waals surface of **NiBi** in **Figure 6**. Instead of the NO_2-moiety, in certain cases the OCH_3-group might interact with the water-subphase, thus causing an inverse orientation, as shown in **Figure 6** for a dimer of **NiBi** with opposing molecular orientations. The structural motive of **NiBi** causes a single condensed phase (A_0 = 33 Å²) that reaches exceptionally high surface pressures and relatively low compressibilities as compared to other thiazoles amphiphiles[42] (compressibility modulus reaching ≈100 mN/m, as shown in Figure SI 64). As clearly visible from the sharp maximum in the compressibility modulus at 27 Å², the monolayer starts transforming into multilayers at 27 Å² (between 40 and 45 mN/m). Again,

further modification of Y by attaching SO_3H (**NiBiSulf**) significantly shifts the isotherm's onset to smaller areas (A_0 = 21 Å²) and induces a liquid phase, as characterized by the small slope between 0 and 10 mN/m. Because of the additional strong anchor, the tendency of monolayer collapse decreases.

It was shown, that the methyl (**Me**) functionalized thiazoles are not sufficient amphiphilic for the Langmuir technique, whereas the extension of the π-system (**Br**, **Bi**) increases the weight of the nonpolar moiety and stabilizes the film formation. Here, the pyridyl (**Py**), but first and foremost the $(CH_3)_2N$ (**Am**) substituent works as a second anchor to the water subphase and enables vertically tilted supramolecular structures. Though appearing to be a predestined second anchor as well, the NO_2 (**Ni**) changes the supramolecular structure distinctly, as such derivatives form dipolar aggregates, which have presumably H-type character, as deduced from the absorption and emission spectra above. Those interactions have been recently shown to significantly stabilize two-dimensional Langmuir layers.[45] Further insights into the supramolecular structure are gained directly during the Langmuir-process *via* online fluorescence monitoring, as detailed below.

In situ Steady State Fluorescence Spectroscopy

Intermolecular interactions between the thiazoles will basically involve dipolar interactions, particularly in case of the push-pull substitutions pattern and ππ-quadrupole or London dispersion interactions in case of the π-extended chromophores. Because the balance between these interactions depends on the polarity of the surrounding medium we have chosen toluene, chloroform, and methanol as prototype non-polar, medium and highly polar solvents, respectively. These solvents might be suitable model-media to mimic different molecular assemblies at hetero-interfaces, as used in the Langmuir technique. In the following we employ UV-vis transmission and emission spectroscopy to dissolved thiazoles to obtain reference spectra to be compared with those of typical H-, J-, or π-aggregates that possibly form at the air-water interface.

The supramolecular structure in the Langmuir layers of different types of 4-hydroxy-5-Y-1,3 thiazoles are characterized by their fluorescence spectra detected *in situ* upon compression. In the following, representative emission spectra of the quasi-gas (negligible molecular interactions) to condensed phases (strong molecular interactions) are compared with solution spectra to determine possible spectral changes arising from intermolecular interactions in the supramolecular assemblies.

4-N,N-Dimethylaminophenyl Derivatives

As compared to the fluorescence spectra of dissolved **AmBr**, the fluorescence spectra of the corresponding Langmuir layers are red-shifted and actually vibrationally not resolved at all investigated surface pressures (see **Figure 7**; for spectra of systematically varied Π see Figure SI 51). The disappearance of the vibronic progression as compared to solution is assigned to a superposition of fluorescence spectra from dyes in slightly varied environments in Langmuir layer within the measurement spot. The red-shift is assigned to the transition from solution to the condensed state. Upon increasing Π, *i.e.* transition from the gas- to the liquid-phase, the emission maximum of **AmBr** shifts slightly red (λ_{max} = 518 nm, Π = 0.1mN/m), followed by a continuous blue-shift (λ_{max} = 500 nm, Π = 12mN/m) in the condensed phase without a change in spectral shape after the collapse point (Π_C > 11 mN/m; for *in situ* fluorescence isotherms shown in SI). The above discussed possible presence of acid-base equilibrium is not reflected in the *in situ* fluorescence spectra. No blue-shifted emission that can be assigned to a protonated species (Figure SI 49) is observed (see Figure SI 51).

In contrast to **AmBr**, Langmuir layers of **AmBi** can be compressed to higher surface pressures, assigned above to a second condensed phase, which gives rise to better resolved vibrational progression see (**Figure 7**, Figure SI 52). The latter indicates improved supramolecular order favored through the extended π-electron system in **AmBi** as compared to **AmBr**. In contrast, the fluorescence spectra of **AmBiSulf** show no dependence on Π (**Figure 7**), hence pointing to a smaller supramolecular order than in case of **AmBi** and possibly a preaggregation in solution or instantly at the air-water interface.

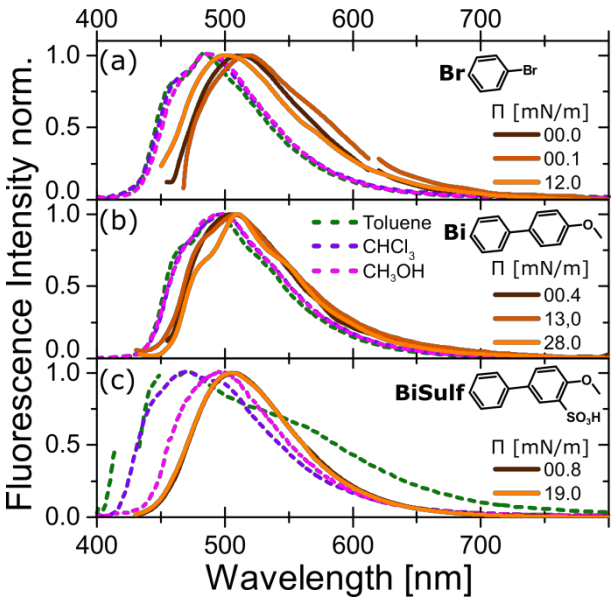

Figure 7: Normalized emission spectra of Langmuir layers at air-water interfaces (solid lines; quasi-2D-phases varied from gas (Π=0 mN/m), to condensed (Π>0 mN/m)) of the 2-(4-N,N-dimethyl-aminophenyl)-4-hydroxy-5-Y-1,3 thiazole core (λ_{exc} = 405 nm) and the phenyl-4-bromo (**AmBr**), phenyl-4-methoxyphenyl (**AmBi**) and 3-phenyl-4-methoxyphenyl-3-sulfonylphenyl (**AmBiSulf**) functionalization and solvent spectra (dashed line) for toluene (dark green), $CHCl_3$ (violet), CH_3OH (pink)

2-Pyridyl Derivatives

Similar to **Am**(**Br**,**BiSulf**) the fluorescence spectra of the Langmuir layers of **Py**(**Br**,**BiSulf**) are slightly red-shifted as compared to the corresponding solutions, show no vibrational progression, and are independent from Π. Again, no spectral sign of protonation (see Figure SI 50) of the basic anchoring group (now pyridine) by the COOH moiety is observed (see **Figure 8**; Figure SI 55). However, **PyBi** shows significant extension of the fluorescence spectra to the red when reaching the condensed phase I, as shown in **Figure 8**.

Difference fluorescence spectra of the **PyBi** Langmuir layers (see Figure SI 56), where the quasi-gas phase spectrum (A = 502 Å²) was subtracted from the remaining spectra, reveal an initial fluorescence decrease for areas shrinking from 800 to 500 Å², followed by a steady fluorescence gain upon further compression into the condensed phases. Consequently, aggregation yields the extension of the fluorescence spectra to the red upon increasing Π reported in **Figure 8**: As revealed by the evolution of the fluorescence difference spectra, aggregates have also formed initially at spreading the chloroform solution of **PyBi**, which dissociate in the course of the LB-experiment provided operation in the quasi-gas-phase. Because of the red-shift, aggregates are assigned as J-type.

As alternative origins of the red-shifted fluorescence peak, one might consider intra- or intermolecular protonation of the pyridine moiety by the COOH acid (λ_{em}=492 nm (neutral),

λ_{em}=622 nm (protonated), see Figure SI 50), or excimer emission[43, 75], which both might change with Π as the supramolecular structures are changing. However, it appears unlikely that such process would be exclusively observed for **PyBi**, but not for all other **Py**-derivatives.

Similar to **PyBr** (which also features similar A_0 areas), the fluorescence spectra of **PyBiSulf** are independent on Π, red-shifted and show no vibronic progression as compared to the solution spectra. These equal results for distinctly different amphiphiles (two as compared to three anchors for **PyBr** and **PyBiSulf**) and the very small A_0 areas imply formation of amorphous rather than well-defined supramolecularly structured films that possibly extent to the third spatial dimension rather than being quasi-two-dimensional prototype Langmuir layers.

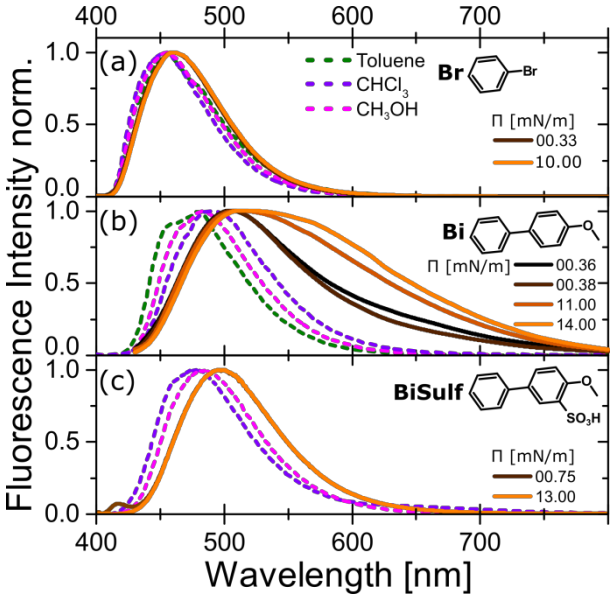

Figure 8: Normalized emission spectra of Langmuir layers at air-water interfaces (solid lines; quasi-2D-phases varied from gas (Π=0 mN/m), to condensed (Π>0 mN/m)) of the 2-(2-pyridyl)-4-hydroxy-5-Y-1,3 thiazole core (λ_{exc} = 405 nm) and the phenyl-4-bromo (**Br**), phenyl-4-methoxyphenyl (**Bi**) and 3-phenyl-4-methoxyphenyl-3-sulfonylphenyl (**BiSulf**) functionalization with the solvent spectra (dashed line) in toluene (dark green), $CHCl_3$ (violet), CH_3OH (pink)

4-Nitrophenyl Derivatives

The fluorescence spectra of **Ni**-derivatives on the LB trough are significantly broader than the spectra of the different solutions discussed above and shown for reference as dashed lines in **Figure 9**. Furthermore, their shape and spectral position typically depends stronger on Π than in case of the **Am**- and **Py**-derivatives discussed above, as surveyed in **Figure 9**.

In detail, the Langmuir layer of the CH_3-functionalized core (**NiMe**) shows a single emission feature (547 nm) located between the emission of maxima obtained for the rather nonpolar toluene and the polar $CHCl_3$-soultions (see **Figure 9**). The emission maximum shifts red (28 nm, Π = 9mN/m; 10 nm, Π = 14mN/m) when probing the compressible monolayer.

The opposite trend is observed for the Langmuir layer made from Y=4-bromophenyl functionalized molecule (**NiBr**). The main emission feature of the Langmuir layer disappears when probing the compressible monolayer and an additional blue-shifted band rises upon increasing Π. Hence, the shape of emission switches from one representing the monomeric emission known from the $CHCl_3$-solution to an H-type aggregate emission (see CH_3OH-solution, **Figure 9**). The latter (λ_{em}=550 nm) features a pronounced vibrionic progression what further supports the assumption of H-aggregate formation. For this aggregation each second **NiBr** dye needs to switch orientation if they were uniquely aligned in the Langmuir gas phase. This reorganization likely causes the dip in the Π(A) isotherm discussed above. The accompanied complex supramolecular and morphological rearrangements during lateral compression of the Langmuir layer likely causes the non-monotonous development of the ratio between monomer and aggregate fluorescence peaks, as seen in **Figure 9** and in Figure SI 59. Formation of a layer over time without lateral compression apparently avoids reorganization in a dense layer and might be understood as crystallization, as the fluorescence spectrum gets smoothly converted from the monomer spectrum to the aggregate spectrum within 40 min (see Figure SI 60). Such time is actually granted during the LB-online-fluorescence measurements. The Π(A) isotherms recorded during these fluorescence measurements ($\Pi(A)^{fluor}$) therefore differ from those discussed above (compare **Figure 6** and Figure SI 59). The $\Pi(A)^{fluor}$ isotherm in Figure SI 59 is shifted to an unphysically small A_0 area, thus indicating growth of H-aggregates in three spatial dimensions, *i.e*. losing the 2D-growth restriction typically enforced by the Langmuir technique in case of **NiBr**.

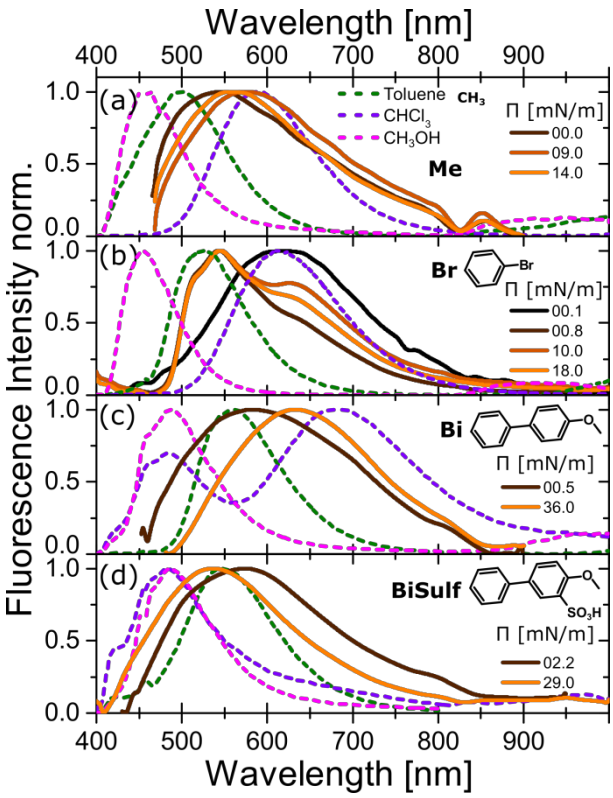

Figure 9: Normalized emission spectra of Langmuir layers at air-water interfaces (solid lines; quasi-2D-phases varied from gas (Π=0 mN/m), to condensed (Π>0 mN/m)) of the 2-(4-nitrophenyl)-4-hydroxy-5-Y-1,3 thiazoles core (λ_{exc} = 405 nm) and the methyl (**Me**), phenyl-4-bromo (**Br**), phenyl-4-methoxyphenyl (**Bi**) and 3-phenyl-4-methoxyphenyl-3-sulfonylphenyl (**BiSulf**) functionalization with the solvent spectra (dashed line) in toluene (dark green), $CHCl_3$ (violet), CH_3OH (pink)

In contrast to **NiBr**, **NiBi** shows just a red-shifted fluorescence (52 nm, 0.175 eV) upon lateral compression from the gas (0.5 mN/m) to the condensed phase (36 mN/m), without appearance of new peaks. Hence, we deduce that the extension of the π-system in **NiBi**, as compared to **NiBr**, hampers reorganization because of increased ππ-interactions, which stabilize a unique molecular orientation within the supramolecular structure. Within such structure the molecules are apparently slightly tilted to additionally stabilize the supramolecular structure *via* J-type dipolar assembly of the D-π-A dyes, as revealed by the successive red-shift upon increasing Π. The avoided reorganization due to stabilization of the two-dimensional layer upon enhanced ππ- and dipolar interactions is presumably the major reason for reaching the exceptionally large surface pressures (Π≈45 mN/m) before reorganization of the monolayer is observed, as discussed above. However, presumably the Langmuir layer consists of small domains, as no vibrational progression can be observed in the Langmuir layer fluorescence.

Contrary to **NiBi**, the fluorescence maximum of the Langmuir layer of **NiBiSulf** (λ_{max} = 574 nm) in the liquid phase (2.2 mN/m) shifts continuously blue (38 nm, 0.149 eV, 29.00 mN/m), what is indicative for the formation of H-aggregates. The reorganization involved in H-aggregate formation (discussed

above for **NiBr**), the high compressibility deduced from the Π(A) isotherms in **Figure 6**, and the unphysically small A_0 areas indicate formation of three-dimensional aggregates upon lateral compression in the Langmuir experiment.

CONCLUSION

In the present work we systematically investigate the influence of the chromophore within the recently introduced class of double-anchor T-shaped amphiphilic dyes[41] on the supramolecular structures they form on the air-water interface in Langmuir experiments. One hydrophilic subphase anchor is provided by a COOH moiety that is centrally linked *via* an alkylic flexible chain to the chromophore's core, namely a 4-hydroxy-thiazole. The second anchor is chosen to be integral part of the chromophore to enable tuning of the molecular orientation upon lateral compression of Langmuir monolayers employed in this work. These R1-anchors in the 2-position of the thiazole have been chosen as 4-N,N-dimethylaminophenyl (**Am**), 2-pyridyl (**Py**), and 4-nitrophenyl (**Ni**).[54, 55] For each of these derivatives, the chromophores have been systematically extended in the 5-position by replacing the methyl (**Me**) moiety with a 4-bromophenyl (**Br**), 4-methoxybiphenyl (**Bi**), and a 4-methoxyphenyl-3-sulfonylphenyl (**BiSulf**) moiety.

As revealed by standard UV-vis transmission and fluorescence spectroscopy on solutions the **Am**-moiety dominates the electronic properties of all investigated **Am**-derivatives. In contrast, the absorption and emission spectra systematically shift red upon extension of the π-system in case of the **Py**- and **Ni**-derivatives.

For the given set of substituents in the 5-position of the thiazole, *i.e*. **Me**, **Br**, **Bi**, **BiSulf**, just the **Ni**-derivatives, essentially **NiBr** and **NiBi**, feature dipolar chromophores that give rise to the formation of H- and J-aggregates at the air-water interface, respectively, as revealed by *in situ* fluorescence spectroscopy performed online during Langmuir experiments. From the Π(A) isotherms and the *in situ* detected fluorescence spectra we deduce reorganization of the **NiBr** dyes and 3D- instead of 2D-growth of their supramolecular structures. In contrast, we find that the diphenylene moiety in **NiBi** significantly stabilizes the compressible monolayer formed by the assembly at the air-water interface. Thus, reorientation is essentially hampered and the dyes form J-aggregates upon lateral compression of the Langmuir layer. The joint stabilization of this **NiBi** layer by ππ- and dipolar interactions gives rise to considerably high surface pressures of ≈45 mN/m[42, 44, 45, 76, 77, 78, 79, 80] that are obtained without any signs of disturbance of the monolayer.

In summary, the combination of the Langmuir technique with online fluorescence measurements revealed that the ππ-interactions, which are pronounced for the **Bi**-derivatives, yield the most

distinct supramolecular structures: While in case of **PyBi** and **NiBi** ordered J-type supramolecular structures in microdomains are formed, as revealed by not vibrationally resolved, red-shifted fluorescence spectra, **AmBi** forms ordered supramolecular structures that are more homogeneous, as revealed by the resolved vibrational progression in the fluorescence spectra, which are, however, not stabilized by J-type dipolar interactions. Hence, the presented systematic study on the influence of the chromophore on the supramolecular structures that form at the air-water interface enables distinct choices of the substitution pattern to target distinct supramolecular structures desired in optoelectronically active materials.

UV-vis Absorption and Fluorescence Spectroscopy

For the absorption spectroscopic measurements, a UV-vis (Varian: Cary 5000) spectrometer was used in transmission mode. The fluorescence measurements using excitation wavelengths larger than 400 nm were performed on a custom built setup (as detailed below), for excitation wavelengths smaller than 400 nm a different spectrometer (Horiba Fluorolog) was used. The Extinction coefficients ($\varepsilon(\lambda_{max})$) of the absorption maxima were calculated *via* linear regression over the concenctration range from $c = 10^{-4}$ M to 10^{-7} M.

LB-Isotherms and *in situ* Fluorescence Spectroscopy of Langmuir layers

For the basic Π(A)-isotherm characterizations solutions of the dyes (1 and 0.1 µmol/ml in 80% $CHCl_3$/ 20% CH_3OH) were carefully spread onto the subphase (ultra-pure water) of the LB-trough (KSV 5000). For complete evaporation a time of 10 min were granted before moving the barriers. Then, the barriers were compressed with a speed of 5 mm/min to record the isotherms.

For the *in situ* fluorescence spectroscopy studies the same Langmuir parameters were applied at a KSV NIMA Alternate L 105 LB trough equipped with a custom-built fluorescence setup. This setup consists of an Isoplane 320 spectrograph with a cooled Pixis CCD-samera from Princeton Instruments. A fiber coupled 5 mW laser with a 405 nm output wavelength was used as excitation source (incident under 55°) and the emission were detected under 0° to the normal. Long pass filters with low self-fluorescence (obtained from ITOS) were used to block scattered excitation light. The data were corrected by a self-written LabView and C++ program. These programs remove remaining scattered excitation light and cosmic rays. The maxima of the fluorescence spectra were analyzed by a self-written Mathematica program.

Density functional theory calculations

Quantum chemical structure optimizations and calculations of electrostatic potential and absorption spectra on **5_5** and **7** monomers were performed using density functional theory (DFT) and its time-

dependent derivative (TD-DFT) as implemented in Turbomole[81] and applying the GGA (generalized gradient approximation) functional BP86 (preoptimization), followed by the hybrid functionals and B3LYP[82], the def2-SVP (preoptimization) and -TZVP basis sets[83], and the MARI-J approximation in case of BP86, which have been shown to yield reasonable electronic properties for a large variety of molecular motives, including push-pull systems and extended π-electron systems[37, 40, 84, 85, 86].

SUPPORTING INFORMATION

The synthesis, used materials, quantum chemically calculated absorption spectra of various conformers, detailed fluorescence spectral series, protonation studies, and further details are provided in the supporting information.

ACKNOWLEDGEMENT

The authors would like to thank the German Research Foundation (DFG PR 1415/2) and Bundesministerium für Bildung und Forschung (BMBF FKZ 03EK3507) for financial support. J.P. acknowledges funding from the Nagelschneider Stiftung.

REFERENCES

1. Mishra, A.; Bäuerle, P. Small Molecule Organic Semiconductors on the Move: Promises for Future Solar Energy Technology. *Angewandte Chemie International Edition* **2012,** *51* (9), 2020-2067.
2. Jou, J.-H.; Kumar, S.; Agrawal, A.; Li, T.-H.; Sahoo, S. Approaches for Fabricating High Efficiency Organic Light Emitting Diodes. *Journal of Materials Chemistry C* **2015,** *3* (13), 2974-3002.
3. Sirringhaus, H. 25th Anniversary Article: Organic Field-Effect Transistors: The Path Beyond Amorphous Silicon. *Advanced Materials* **2014,** *26* (9), 1319-1335.
4. Das, S.; Herrmann-Westendorf, F.; Schacher, F. H.; Tauscher, E.; Ritter, U.; Dietzek, B.; Presselt, M. Controlling Electronic Transitions in Fullerene van der Waals Aggregates via Supramolecular Assembly. *ACS Applied Materials & Interfaces* **2016,** *8* (33), 21512-21521.
5. Herrmann, F.; Engmann, S.; Presselt, M.; Hoppe, H.; Shokhovets, S.; Gobsch, G. Correlation between near infrared-visible absorption, intrinsic local and global sheet resistance of poly(3,4-ethylenedioxy-thiophene) poly(styrene sulfonate) thin films. *Applied Physics Letters* **2012,** *100* (15), 153301-01 - 03.
6. Gampe, D. M.; Nöller, F.; Hänsch, V. G.; Schramm, S.; Darsen, A.; Habenicht, S. H.; Ehrhardt, S.; Weiß, D.; Görls, H.; Beckert, R. Surprising characteristics of D–A-type functional dyes by introducing 4-alkoxythiazoles as the donor-unit. *Tetrahedron* **2016,** *72* (23), 3232-3239.
7. Würthner, F.; Kaiser, T. E.; Saha-Möller, C. R. J-Aggregates: From Serendipitous Discovery to Supramolecular Engineering of Functional Dye Materials. *Angewandte Chemie International Edition* **2011,** *50* (15), 3376-3410.
8. Biesmans, G.; Verbeek, G.; Verschuere, B.; van der Auweraer, M.; De Schryver, F. C. On the fluorescence of anthracene chromophores in langmuir-blodgett films. *Thin Solid Films* **1989,** *169* (1), 127-142.

9. Flämmich, M.; Gather, M. C.; Danz, N.; Michaelis, D.; Bräuer, A. H.; Meerholz, K.; Tünnermann, A. Orientation of Emissive Dipoles in OLEDs: Quantitative In Situ Analysis. *Organic Electronics* **2010,** *11* (6), 1039-1046.
10. Mayr, C.; Schmidt, T. D.; Brütting, W. High-efficiency fluorescent organic light-emitting diodes enabled by triplet-triplet annihilation and horizontal emitter orientation. *Applied Physics Letters* **2014,** *105* (18), 183304-01 - 04.
11. Presselt, M.; Herrmann, F.; Hoppe, H.; Shokhovets, S.; Runge, E.; Gobsch, G. Influence of Phonon Scattering on Exciton and Charge Diffusion in Polymer-Fullerene Solar Cells. *Advanced Energy Materials* **2012,** *2* (8), 999-1003.
12. Beenken, W. J. D.; Herrmann, F.; Presselt, M.; Hoppe, H.; Shokhovets, S.; Gobsch, G.; Runge, E. Sub-bandgap absorption in organic solar cells: experiment and theory. *Physical Chemistry Chemical Physics* **2013,** *15* (39), 16494-16502.
13. Presselt, M.; Bärenklau, M.; Rösch, R.; Beenken, W. J. D.; Runge, E.; Shokhovets, S.; Hoppe, H.; Gobsch, G. Sub-Bandgap Absorption in Polymer-Fullerene Solar Cells. *Applied Physics Letters* **2010,** *97* (25), 253302-01 - 02.
14. Shewmon, N. T.; Watkins, D. L.; Galindo, J. F.; Zerdan, R. B.; Chen, J.; Keum, J.; Roitberg, A. E.; Xue, J.; Castellano, R. K. Enhancement in Organic Photovoltaic Efficiency Through the Synergistic Interplay of Molecular Donor Hydrogen Bonding and π-Stacking. *Advanced Functional Materials* **2015,** *25* (32), 5166-5177.
15. Li, Z.; Bian, J.; Wang, Y.; Jiang, F.; Liang, G.; He, P.; Hou, Q.; Tong, J.; Liang, Y.; Zhong, Z.; Zhou, Y.; Tian, W. Effect of Alkyl Chain Length on the Photovoltaic Performance of Oligothiophene-Based Small Molecules. *Solar Energy Materials and Solar Cells* **2014,** *130*, 336-346.
16. Poelking, C.; Tietze, M.; Elschner, C.; Olthof, S.; Hertel, D.; Baumeier, B.; Würthner, F.; Meerholz, K.; Leo, K.; Andrienko, D. Impact of mesoscale order on open-circuit voltage in organic solar cells. *Nat Mater* **2015,** *14* (4), 434-439.
17. Chen, Y.; Feng, Y.; Gao, J.; Bouvet, M. Self-Assembled Aggregates of Amphiphilic Perylene Diimide–Based Semiconductor Molecules: Effect of Morphology on Conductivity. *Journal of Colloid and Interface Science* **2012,** *368* (1), 387-394.
18. Grozema, F. C.; Siebbeles, L. D. A. Mechanism of Charge Transport in Self-Organizing Organic Materials. *Int. Rev. Phys. Chem.* **2008,** *27* (1), 87-138.
19. Wang, S.; Fabiano, S.; Himmelberger, S.; Puzinas, S.; Crispin, X.; Salleo, A.; Berggren, M. Experimental evidence that short-range intermolecular aggregation is sufficient for efficient charge transport in conjugated polymers. *Proceedings of the National Academy of Sciences* **2015,** *112* (34), 10599-10604.
20. Presselt, M.; Herrmann, F.; Shokhovets, S.; Hoppe, H.; Runge, E.; Gobsch, G. Sub-bandgap absorption in polymer-fullerene solar cells studied by temperature-dependent external quantum efficiency and absorption spectroscopy. *Chemical Physics Letters* **2012,** *542*, 70-73.
21. Kar, H.; Gehrig, D. W.; Laquai, F.; Ghosh, S. J-Aggregation, its Impact on Excited State Dynamics and Unique Solvent Effects on Macroscopic Assembly of a Core-Substituted Naphthalenediimide. *Nanoscale* **2015,** *7* (15), 6729-6736.
22. Wong, C. Y.; Penwell, S. B.; Cotts, B. L.; Noriega, R.; Wu, H.; Ginsberg, N. S. Revealing Exciton Dynamics in a Small-Molecule Organic Semiconducting Film with Subdomain Transient Absorption Microscopy. *The Journal of Physical Chemistry C* **2013,** *117* (42), 22111-22122.
23. De la Cadena, A.; Pascher, T.; Davydova, D. y.; Akimov, D.; Herrmann, F.; Presselt, M.; Wächtler, M.; Dietzek, B. Intermolecular exciton–exciton annihilation in phospholipid vesicles doped with [Ru(bpy)2dppz]2+. *Chemical Physics Letters* **2016,** *644*, 56-61.
24. Kitchen, B.; Awartani, O.; Kline, R. J.; McAfee, T.; Ade, H.; O'Connor, B. T. Tuning Open-Circuit Voltage in Organic Solar Cells with Molecular Orientation. *Acs Applied Materials & Interfaces* **2015,** *7* (24), 13208-13216.
25. Zhong, S.; Zhong, J. Q.; Wee, A. T. S.; Chen, W. Molecular Orientation and Electronic Structure at Organic Heterojunction Interfaces. *Journal of Electron Spectroscopy and Related Phenomena* **2015,** *204*, 12-22.

26. Bürckstümmer, H.; Tulyakova, E. V.; Deppisch, M.; Lenze, M. R.; Kronenberg, N. M.; Gsänger, M.; Stolte, M.; Meerholz, K.; Würthner, F. Efficient Solution-Processed Bulk Heterojunction Solar Cells by Antiparallel Supramolecular Arrangement of Dipolar Donor–Acceptor Dyes. *Angewandte Chemie International Edition* **2011,** *50* (49), 11628-11632.
27. Herrmann-Westendorf, F.; Sachse, T.; Schulz, M.; Kaufmann, M.; Sivakov, V.; Beckert, R.; Martinez, T. J.; Dietzek, B.; Presselt, M. Photo-Annealing of Merocyanine Aggregates. *The journal of physical chemistry. A* **2018**.
28. Würthner, F.; Chen, Z. J.; Hoeben, F. J. M.; Osswald, P.; You, C. C.; Jonkheijm, P.; von Herrikhuyzen, J.; Schenning, A.; van der Schoot, P.; Meijer, E. W.; Beckers, E. H. A.; Meskers, S. C. J.; Janssen, R. A. J. Supramolecular p-n-heterojunctions by co-self-organization of oligo(p-phenylene vinylene) and perylene bisimide dyes. *Journal Of The American Chemical Society* **2004,** *126* (34), 10611-10618.
29. Ariga, K.; Hill, J. P.; Ji, Q. Layer-By-Layer Assembly as a Versatile Bottom-Up Nanofabrication Technique for Exploratory Research and Realistic Application. *Physical Chemistry Chemical Physics* **2007,** *9* (19), 2319-2340.
30. Wang, Y.; Angelatos, A. S.; Caruso, F. Template Synthesis of Nanostructured Materials via Layer-by-Layer Assembly. *Chemistry of Materials* **2008,** *20* (3), 848-858.
31. Modlińska, A.; Piosik, E.; Paluszkiewicz, J.; Martyński, T. Aggregation properties of tetrachloroperylene-tetracarboxylic acid in binary Langmuir and Langmuir–Blodgett films. *J. Lumin.* **2014,** *148*, 44-54.
32. Angelova, A.; Ionov, R. Monolayer and Spectroscopic Studies of an Amphiphilic (Phenylethynyl)anthracene Probe in Pure and Mixed Films with Charged and Neutral Lipids. *Langmuir* **1999,** *15* (21), 7199-7207.
33. Modlińska, A.; Bauman, D. The Langmuir-Blodgett Technique as a Tool for Homeotropic Alignment of Fluorinated Liquid Crystals Mixed with Arachidic Acid. *International Journal of Molecular Sciences* **2011,** *12* (8), 4923-4945.
34. Ariga, K.; Yamauchi, Y.; Mori, T.; Hill, J. P. 25th Anniversary Article: What Can Be Done with the Langmuir-Blodgett Method? Recent Developments and its Critical Role in Materials Science. *Advanced Materials* **2013,** *25* (45), 6477-6512.
35. Jin, J.; Li, L. S.; Li, Y.; Zhang, Y. J.; Chen, X.; Wang, D.; Jiang, S.; Li, T. J.; Gan, L. B.; Huang, C. H. Structural Characterizations of C60-Derivative Langmuir−Blodgett Films and Their Photovoltaic Behaviors. *Langmuir* **1999,** *15* (13), 4565-4569.
36. Das, S.; Preiß, J.; Plentz, J.; Brückner, U.; von der Lühe, M.; Eckardt, O.; Dathe, A.; Schacher, F. H.; Täuscher, E.; Ritter, U.; Csáki, A.; Andrä, G.; Dietzek, B.; Presselt, M. Controlling Intermolecular Interactions at Interfaces: Case of Supramolecular Tuning of Fullerene's Electronic Structure. *Advanced Energy Materials* **2018,** *8* (32), 1801737.
37. Presselt, M.; Schnedermann, C.; Müller, M.; Schmitt, M.; Popp, J. Derivation of Correlation Functions to Predict Bond Properties of Phenyl-CH Bonds Based on Vibrational and H-1 NMR Spectroscopic Quantities. *Journal of Physical Chemistry A* **2010,** *114* (37), 10287-10296.
38. Fitzner, R.; Mena-Osteritz, E.; Mishra, A.; Schulz, G.; Reinold, E.; Weil, M.; Koerner, C.; Ziehlke, H.; Elschner, C.; Leo, K.; Riede, M.; Pfeiffer, M.; Uhrich, C.; Baeuerle, P. Correlation of pi-Conjugated Oligomer Structure with Film Morphology and Organic Solar Cell Performance. *Journal of the American Chemical Society* **2012,** *134* (27), 11064-11067.
39. Szłapa, A.; Kula, S.; Błaszkiewicz, U.; Grucela, M.; Schab-Balcerzak, E.; Filapek, M. Simple Donor–π–Acceptor Derivatives Exhibiting Aggregation-Induced Emission Characteristics for Use as Emitting Layer in OLED. *Dyes and Pigments* **2016,** *129*, 80-89.
40. Presselt, M.; Schnedermann, C.; Schmitt, M.; Popp, J. Prediction of electron densities, the respective laplacians, and ellipticities in bond-critical points of phenyl-CH-bonds via linear relations to parameters of inherently localized CD stretching vibrations and 1H NMR-shifts. *The journal of physical chemistry. A* **2009,** *113* (13), 3210-22.
41. Hupfer, M. L.; Kaufmann, M.; Herrmann-Westendorf, F.; Sachse, T.; Roussille, L.; Feller, K. H.; Weiss, D.; Deckert, V.; Beckert, R.; Dietzek, B.; Presselt, M. On the Control of Chromophore

Orientation, Supramolecular Structure, and Thermodynamic Stability of an Amphiphilic Pyridyl-Thiazol upon Lateral Compression and Spacer Length Variation. *ACS Appl Mater Interfaces* **2017,** *9* (50), 44181-44191.

42. Kaufmann, M.; Hupfer, M. L.; Sachse, T.; Herrmann-Westendorf, F.; Weiß, D.; Dietzek, B.; Beckert, R.; Presselt, M. Introducing double polar heads to highly fluorescent Thiazoles: Influence on supramolecular structures and photonic properties. *Journal of colloid and interface science* **2018,** *526*, 410-418.

43. Habenicht, S. H.; Schramm, S.; Fischer, S.; Sachse, T.; Herrmann-Westendorf, F.; Bellmann, A.; Dietzek, B.; Presselt, M.; Wei; Beckert, R.; Görls, H. Tuning the polarity and surface activity of hydroxythiazoles - extending the applicability of highly fluorescent self-assembling chromophores to supra-molecular photonic structures. *Journal of Materials Chemistry C* **2016,** *4* (5), 958-971.

44. Hupfer, M. L.; Kaufmann, M.; Roussille, L.; Preiß, J.; Weiß, D.; Hinrichs, K.; Deckert, V.; Dietzek, B.; Beckert, R.; Presselt, M. Arylic vs. Alkylic - Hydrophobic Linkers Determine Supramolecular Structure and Optoelectronic Properties of Tripodal Amphiphilic Push-Pull-Thiazoles. *Langmuir* **2019,** *submitted*.

45. Hupfer, M. L.; Kaufmann, M.; Preiß, J.; Weiß, D.; Dietzek, B.; Beckert, R.; Presselt, M. Combining Dipolar Aggregate Formation with Two-Dimensional Assembly at Air-Water-Interfaces: Case of Amphiphilic Push-Pull-Thiazoles. *Advanced Materials* **2019,** *submitted*.

46. Hupfer, M. L.; Herrmann-Westendorf, F.; Kaufmann, M.; Beckert, R.; Dietzek, B.; Presselt, M. Autonomous Interface Self-Healing: Monitored by Restoration of UV-vis Absorption Spectra of Self-Assembled Thiazole Layers. *Chemistry - A European Journal* **2019,** *submitted*.

47. Ranyuk, E.; Ermakova, E. V.; Bovigny, L.; Meyer, M.; Bessmertnykh-Lemeune, A.; Guilard, R.; Rousselin, Y.; Tsivadze, A. Y.; Arslanov, V. V. Towards sensory Langmuir monolayers consisting of macrocyclic pentaaminoanthraquinone. *New Journal of Chemistry* **2014,** *38* (1), 317-329.

48. Caruso, F.; Grieser, F.; Thistlethwaite, P. J.; Almgren, M. Two-dimensional diffusion of amphiphiles in phospholipid monolayers at the air-water interface. *Biophysical Journal* **1993,** *65* (6), 2493-2503.

49. Grummt, U.-W.; Weiss, D.; Birckner, E.; Beckert, R. Pyridylthiazoles: Highly luminescent heterocyclic compounds. *Journal of Physical Chemistry A* **2007,** *111* (6), 1104-1110.

50. Menzel, R.; Ogermann, D.; Kupfer, S.; Weiß, D.; Görls, H.; Kleinermanns, K.; González, L.; Beckert, R. 4-Methoxy-1,3-thiazole based donor-acceptor dyes: Characterization, X-ray structure, DFT calculations and test as sensitizers for DSSC. *Dyes and Pigments* **2012,** *94* (3), 512-524.

51. Breul, A. M.; Pietsch, C.; Menzel, R.; Schäfer, J.; Teichler, A.; Hager, M. D.; Popp, J.; Dietzek, B.; Beckert, R.; Schubert, U. S. Blue Emitting Side-Chain Pendant 4-Hydroxy-1,3-Thiazoles in Polystyrenes Synthesized by RAFT Polymerization. *Eur. Polym. J.* **2012,** *48* (7), 1339-1347.

52. Menzel, R.; Breul, A.; Pietsch, C.; Schäfer, J.; Friebe, C.; Täuscher, E.; Weiß, D.; Dietzek, B.; Popp, J.; Beckert, R.; Schubert, U. S. Blue-Emitting Polymers Based on 4-Hydroxythiazoles Incorporated in a Methacrylate Backbone. *Macromol. Chem. Phys.* **2011,** *212* (8), 840-848.

53. Usta, H.; Sheets, W. C.; Denti, M.; Generali, G.; Capelli, R.; Lu, S.; Yu, X.; Muccini, M.; Facchetti, A. Perfluoroalkyl-Functionalized Thiazole–Thiophene Oligomers as N-Channel Semiconductors in Organic Field-Effect and Light-Emitting Transistors. *Chemistry of Materials* **2014,** *26* (22), 6542-6556.

54. Cong, J.; Yang, X.; Liu, J.; Zhao, J.; Hao, Y.; Wang, Y.; Sun, L. Nitro group as a new anchoring group for organic dyes in dye-sensitized solar cells. *Chemical Communications* **2012,** *48* (53), 6663-6665.

55. Zhang, L.; Cole, J. M. Anchoring Groups for Dye-Sensitized Solar Cells. *ACS Applied Materials & Interfaces* **2015,** *7* (6), 3427-3455.

56. Calderón-Ortiz, L. K.; Täuscher, E.; Leite Bastos, E.; Görls, H.; Weiß, D.; Beckert, R. Hydroxythiazole-Based Fluorescent Probes for Fluoride Ion Detection. *Eur. J. Org. Chem.* **2012,** *2012* (13), 2535-2541.

57. Wolfram, S.; Wurfel, H.; Habenicht, S. H.; Lembke, C.; Richter, P.; Birckner, E.; Beckert, R.; Pohnert, G. A small azide-modified thiazole-based reporter molecule for fluorescence and mass spectrometric detection. *Beilstein J. Org. Chem.* **2014,** *10*, 2470-9.
58. Menzel, R.; Kupfer, S.; Mede, R.; Weiß, D.; Görls, H.; González, L.; Beckert, R. Arylamine-Modified Thiazoles as Donor–Acceptor Dyes: Quantum Chemical Evaluation of the Charge-Transfer Process and Testing as Ligands in Ruthenium(II) Complexes. *European Journal of Organic Chemistry* **2012,** *2012* (27), 5231-5247.
59. Täuscher, E.; Weiß, D.; Beckert, R.; Fabian, J.; Assumpção, A.; Görls, H. Classical heterocycles with surprising properties: the 4-hydroxy-1,3-thiazoles. *Tetrahedron Letters* **2011,** *52* (18), 2292-2294.
60. Menzel, R.; Täuscher, E.; Weiß, D.; Beckert, R.; Görls, H. The Combination of 4-Hydroxythiazoles with Azaheterocycles: Efficient Bidentate Ligands for Novel Ruthenium Complexes. *Zeitschrift für anorganische und allgemeine Chemie* **2010,** *636* (7), 1380-1385.
61. Kerdesky, F. A. J.; Holms, J. H.; Moore, J. L.; Bell, R. L.; Dyer, R. D.; Carter, G. W.; Brooks, D. W. 4-Hydroxythiazole inhibitors of 5-lipoxygenase. *J. Med. Chem.* **1991,** *34* (7), 2158-2165.
62. Gampe, D. M.; Hänsch, V. G.; Schramm, S.; Menzel, R.; Weiß, D.; Beckert, R. Mixing Chromophores: Donor–Acceptor Dyes with Low-Lying LUMOs and Narrow Band Gaps by Connecting 4-Alkoxythiazoles and Azaacenes. *European Journal of Organic Chemistry* **2017,** *2017* (10), 1369-1379.
63. Habenicht, S. H.; Schramm, S.; Zhu, M.; Freund, R. R.; Langenstuck, T.; Strathausen, R.; Weiss, D.; Biskup, C.; Beckert, R. pi-Extension of a 4-ethoxy-1,3-thiazole via aryl alkyne cross coupling: synthesis and exploration of the electronic structure. *Photochemical & photobiological sciences : Official journal of the European Photochemistry Association and the European Society for Photobiology* **2015,** *14* (11), 2097-107.
64. Arcadi, A.; Attanasi, O. A.; Guidi, B.; Rossi, E.; Santeusanio, S. 2-Substituted 5-Acetyl-4-Thiazolyl Triflates as Useful Building Blocks for the Preparation of Functionalized Thiazoles. *European Journal of Organic Chemistry* **1999,** *1999* (11), 3117-3126.
65. Habenicht, S. H.; Siegmann, M.; Kupfer, S.; Kübel, J.; Weiß, D.; Cherek, D.; Möller, U.; Dietzek, B.; Gräfe, S.; Beckert, R. And yet they glow: thiazole based push–pull fluorophores containing nitro groups and the influence of regioisomerism. *Methods and Applications in Fluorescence* **2015,** *3* (2), 025005.
66. Kaganer, V. M.; Mohwald, H.; Dutta, P. Structure and phase transitions in Langmuir monolayers. *Reviews of Modern Physics* **1999,** *71* (3), 779-819.
67. Villares, A.; Lydon, D. P.; Low, P. J.; Robinson, B. J.; Ashwell, G. J.; Royo, F. M.; Cea, P. Characterization and Conductivity of Langmuir–Blodgett Films Prepared from an Amine-Substituted Oligo(phenylene ethynylene). *Chemistry of Materials* **2008,** *20* (1), 258-264.
68. Sýkora, D.; Tesařová, E.; Popl, M. Interactions of basic compounds in reversed-phase high-performance liquid chromatography influence of sorbent character, mobile phase composition, and pH on retention of basic compounds. *Journal of Chromatography A* **1997,** *758* (1), 37-51.
69. Williams, M. The Merck Index: An Encyclopedia of Chemicals, Drugs, and Biologicals, 15th Edition Edited by M.J. O'Neil , PB - Royal Society of Chemistry , Cambridge, UK ISBN 9781849736701; 2708 pages. April 2013, $150 with 1-year free access to The Merck Index Online. *Drug Development Research* **2013,** *74* (5), 339-339.
70. Herrmann, F.; Muhsin, B.; Singh, C. R.; Shokhovets, S.; Gobsch, G.; Hoppe, H.; Presselt, M. Influence of Interface Doping on Charge-Carrier Mobilities and Sub-Bandgap Absorption in Organic Solar Cells. *The Journal of Physical Chemistry C* **2015,** *119* (17), 9036-9040.
71. Hartman, C. K.; Mezei, G. Mapping the Intricate Reactivity of Nanojars toward Molecules of Varying Acidity and Their Conjugate Bases Leading To Exchange of Pyrazolate Ligands. *Inorganic Chemistry* **2017,** *56* (17), 10609-10624.
72. Nachod, F. C.; Braude, E. A.; Phillips, W. D. *Determination of organic structures by physical methods / editors, E.A. Braude, F.C. Nachod*; Academic Press: New York, 1955.

73. Inglot, K.; Martyński, T.; Bauman, D. Surface potential measurements of Langmuir films of azo dye/liquid crystal mixtures. *Dyes and Pigments* **2009,** *80* (1), 106-114.
74. Dynarowicz; tka, P.; Milart, P. Synthesis and Langmuir monolayer characterisation of some nitro derivatives of polyphenyl carboxylic acids. *Journal of Chemical Research* **2009,** *2009* (4), 225-228.
75. Biadasz, A.; Łabuszewska, K.; Chrzumnicka, E.; Michałowski, E.; Martyński, T.; Bauman, D. Spectral properties of some fluorescent dyes in two-dimensional films formed by means of Langmuir–Blodgett technique. *Dyes and Pigments* **2007,** *74* (3), 598-607.
76. Schwieger, C.; Chen, B.; Tschierske, C.; Kressler, J.; Blume, A. Organization of T-Shaped Facial Amphiphiles at the Air/Water Interface Studied by Infrared Reflection Absorption Spectroscopy. *The Journal of Physical Chemistry B* **2012,** *116* (40), 12245-12256.
77. Das, S.; Preiß, J.; Plentz, J.; Brückner, U.; von der Lühe, M.; Eckardt, O.; Dathe, A.; Schacher, F. H.; Täuscher, E.; Ritter, U.; Csáki, A.; Andrä, G.; Dietzek, B.; Presselt, M. Controlling Intermolecular Interactions at Interfaces: Case of Supramolecular Tuning of Fullerene's Electronic Structure. *Advanced Energy Materials* **2018,** *0* (0), 1801737.
78. Bauman, D.; Hertmanowski, R.; Stefańska, K.; Stolarski, R. The synthesis of novel perylene-like dyes and their aggregation properties in Langmuir and Langmuir–Blodgett films. *Dyes Pigm.* **2011,** *91* (3), 474-480.
79. del Caño, T.; Parra, V.; Rodríguez-Méndez, M. L.; Aroca, R.; de Saja, J. A. Molecular stacking and emission properties in Langmuir–Blodgett films of two alkyl substituted perylene tetracarboxylic diimides. *Organic Electronics* **2004,** *5* (1), 107-114.
80. Zou, L.; You, A.; Song, J.; Li, X.; Bouvet, M.; Sui, W.; Chen, Y. Cation-induced self-assembly of an amphiphilic perylene diimide derivative in solution and Langmuir–Blodgett films. *Colloids and Surfaces A: Physicochemical and Engineering Aspects* **2015,** *465* (Supplement C), 39-46.
81. Ahlrichs, R.; Bär, M.; Häser, M.; Horn, H.; Kölmel, C. Electronic structure calculations on workstation computers: The program system turbomole. *Chemical Physics Letters* **1989,** *162* (3), 165-169.
82. Stephens, P. J.; Devlin, F. J.; Chabalowski, C. F.; Frisch, M. J. Ab-Initio Calculation of Vibrational Absorption and Circular-Dichroism Spectra Using Density-Functional Force-Fields. *The Journal of Physical Chemistry* **1994,** *98* (45), 11623-11627.
83. Weigend, F.; Ahlrichs, R. Balanced basis sets of split valence, triple zeta valence and quadruple zeta valence quality for H to Rn: Design and assessment of accuracy. *Physical Chemistry Chemical Physics* **2005,** *7* (18), 3297-3305.
84. Gampe, D. M.; Kaufmann, M.; Jakobi, D.; Sachse, T.; Presselt, M.; Beckert, R.; Gorls, H. Stable and easily accessible functional dyes: dihydrotetraazaanthracenes as versatile precursors for higher acenes. *Chemistry* **2015,** *21* (20), 7571-81.
85. Preiß, J.; Jäger, M.; Rau, S.; Dietzek, B.; Popp, J.; Martínez, T.; Presselt, M. How Does Peripheral Functionalization of Ruthenium(II)–Terpyridine Complexes Affect Spatial Charge Redistribution after Photoexcitation at the Franck–Condon Point? *ChemPhysChem* **2015,** *16* (7), 1395-1404.
86. Presselt, M.; Dehaen, W.; Maes, W.; Klamt, A.; Martínez, T.; Beenken, W. J. D.; Kruk, M. Quantum Chemical Insights into the Dependence of Porphyrin Basicity on the Meso-Aryl Substituents: Thermodynamics, Buckling, Reaction Sites and Molecular Flexibility. *Physical Chemistry Chemical Physics* **2015,** *17* (21), 14096-14106.

TABLE OF CONTENT

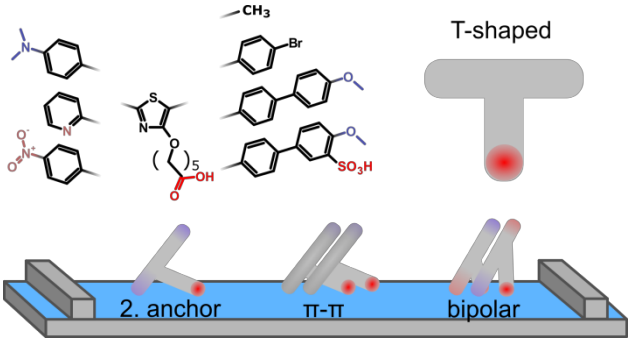

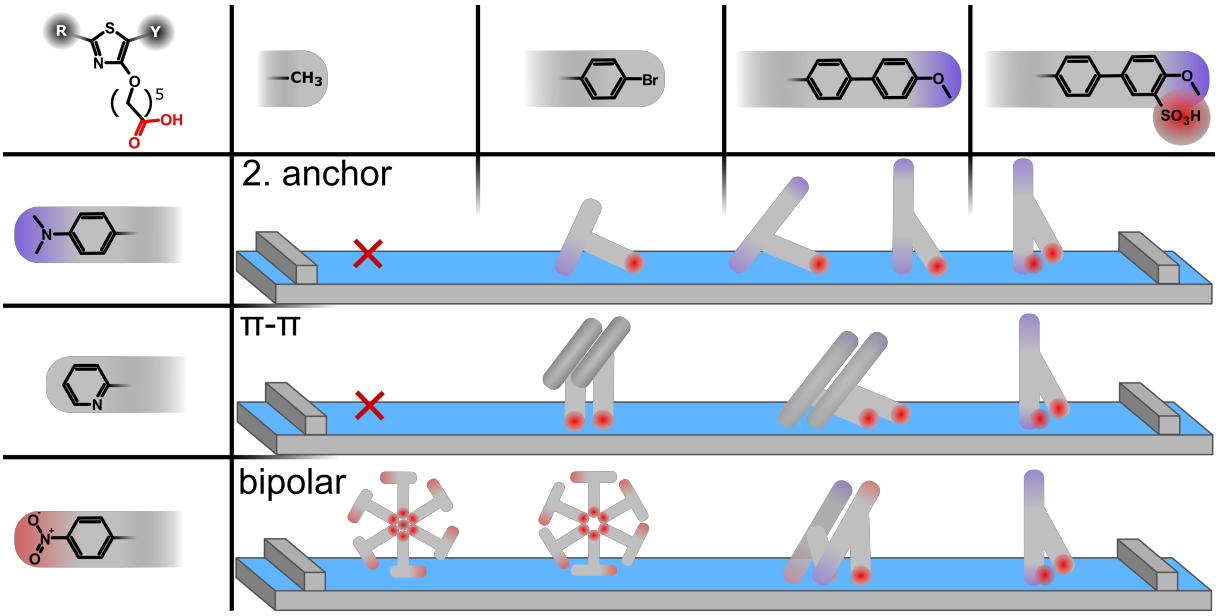
R
S
Y
N
O
5
OH
O
CH3
Br
O
O
SO3H
2. anchor
N
π-π
N
bipolar
N
O
O

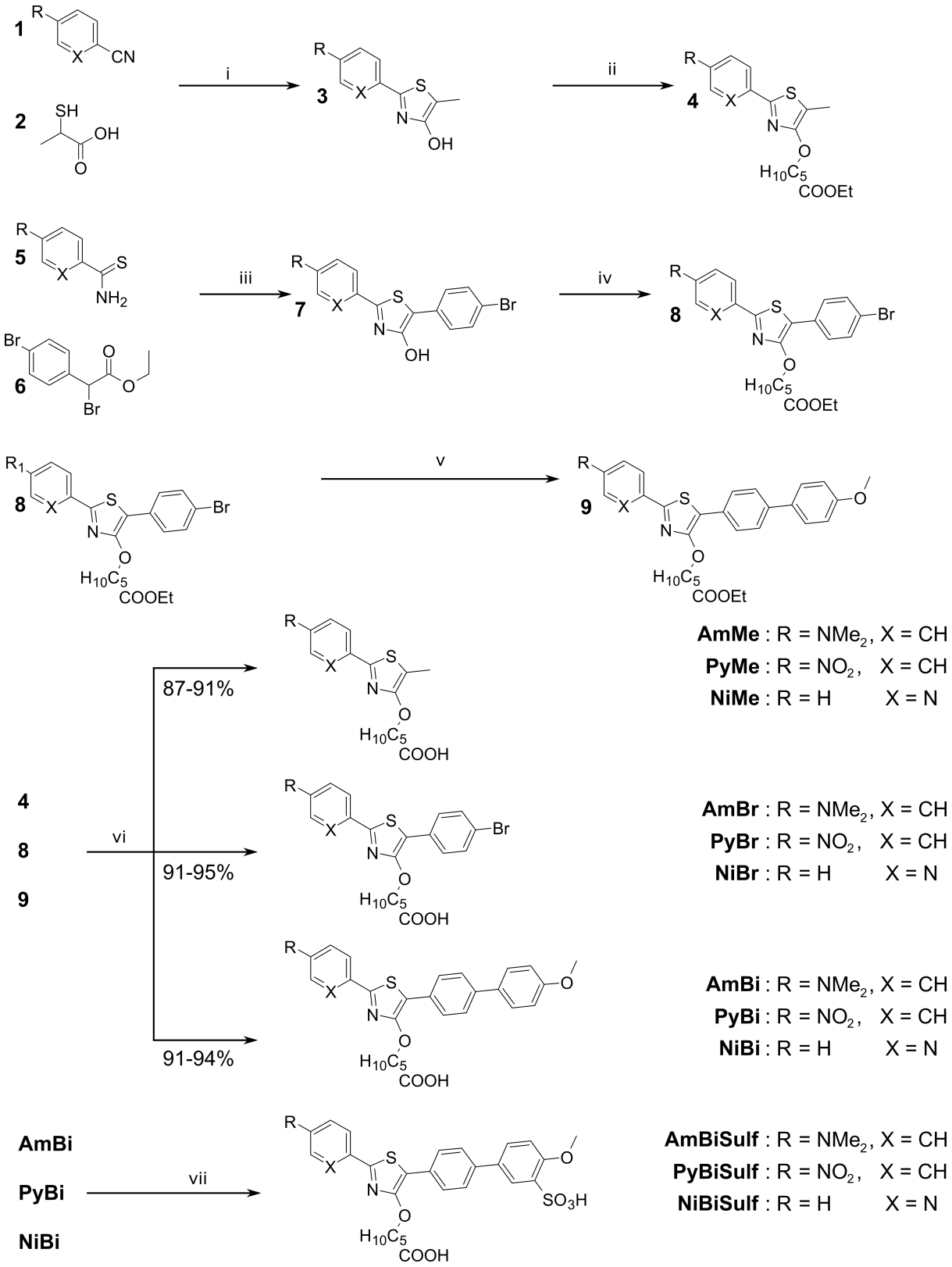
1
2
i
3
ii
4
5
6
iii
7
iv
8
v
9
vi
87-91%
91-95%
91-94%
vii
AmBi
PyBi
NiBi
AmMe : R = NMe2, X = CH
PyMe : R = NO2, X = CH
NiMe : R = H X = N
AmBr : R = NMe2, X = CH
PyBr : R = NO2, X = CH
NiBr : R = H X = N
AmBi : R = NMe2, X = CH
PyBi : R = NO2, X = CH
NiBi : R = H X = N
AmBiSulf : R = NMe2, X = CH
PyBiSulf : R = NO2, X = CH
NiBiSulf : R = H X = N

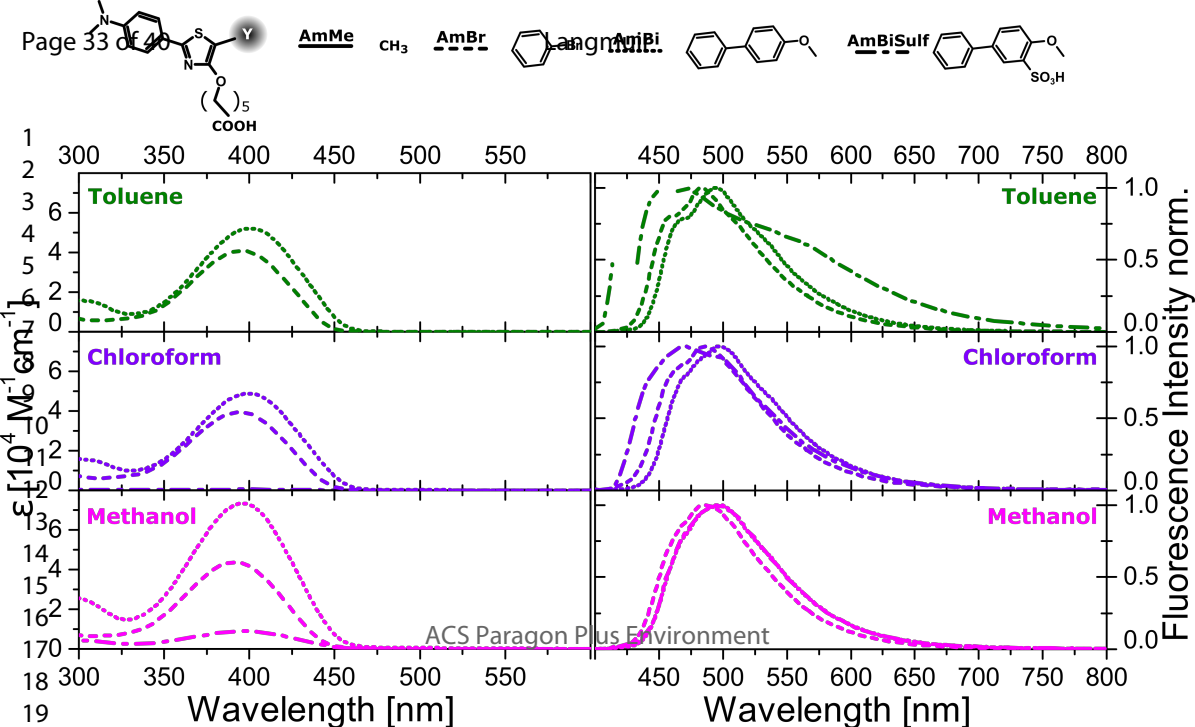
AmMe
AmBr
AmBi
AmBiSulf
COOH
Toluene
Chloroform
Methanol
ε [10^4 M^-1 cm^-1]
Fluorescence Intensity norm.
Wavelength [nm]
Wavelength [nm]
ACS Paragon Plus Environment

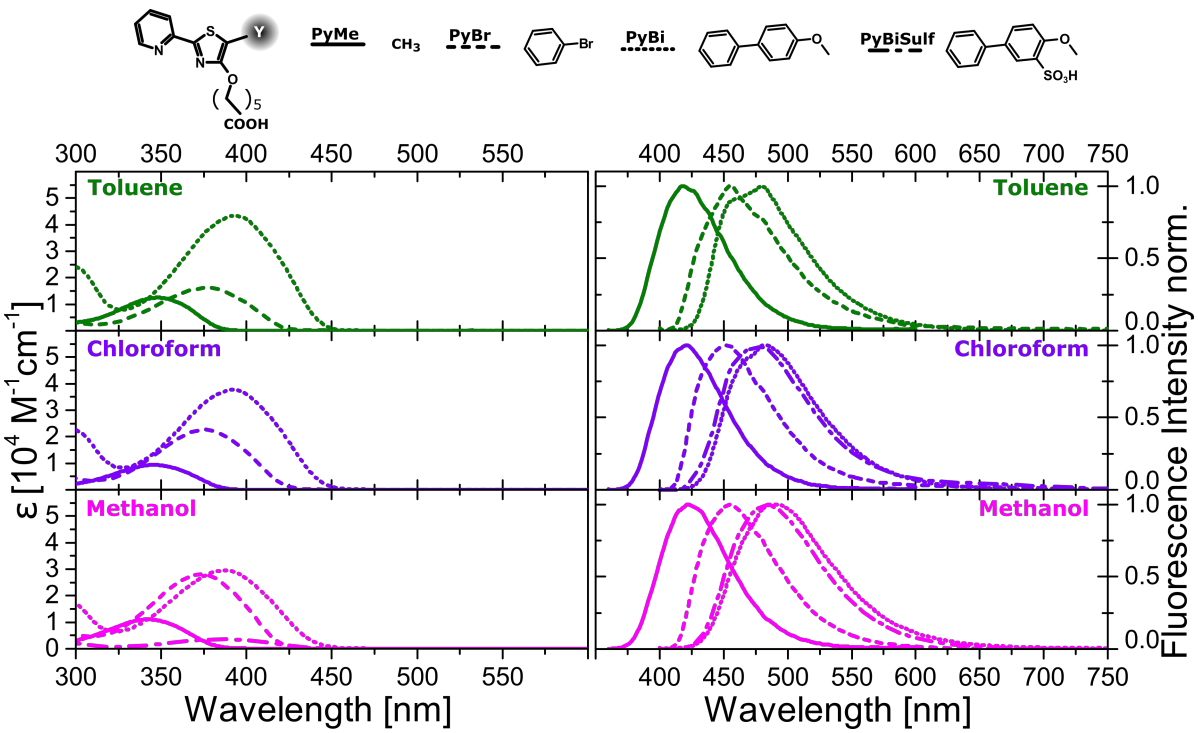
PyMe
CH3
PyBr
Br
PyBi
PyBiSulf
SO3H
COOH
Toluene
Chloroform
Methanol
ε [10^4 M^-1cm^-1]
Fluorescence Intensity norm.
Wavelength [nm]
Wavelength [nm]

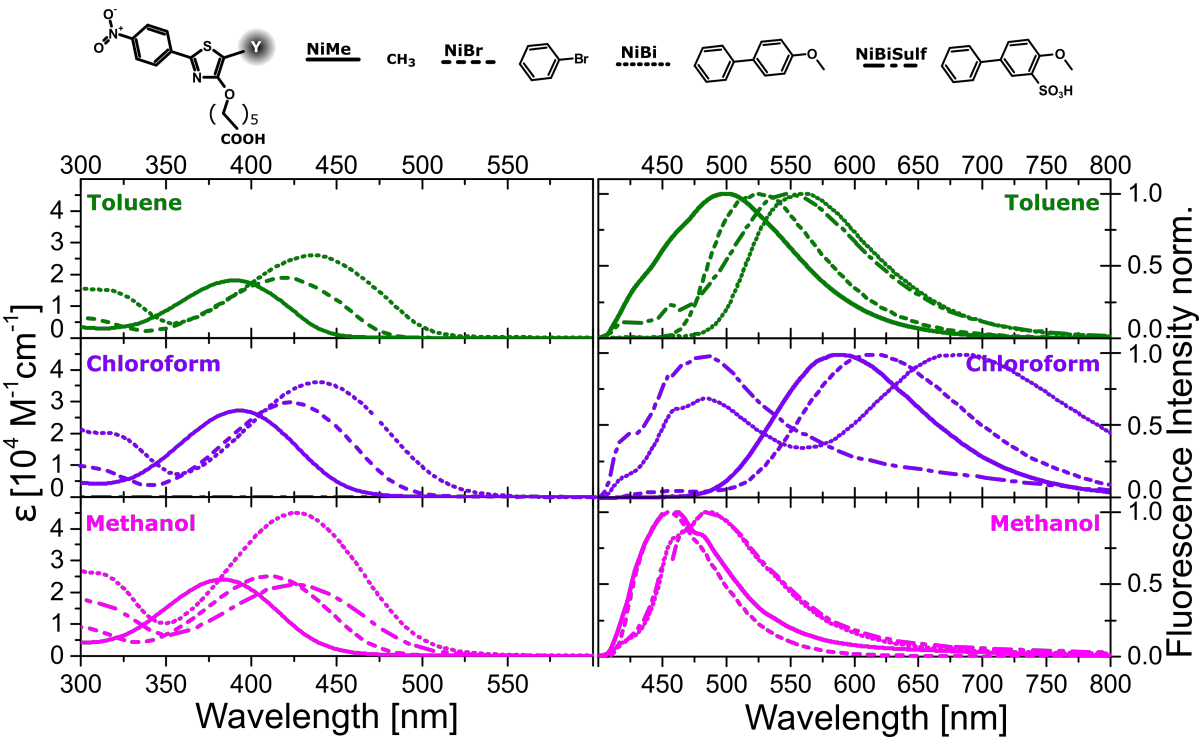
NiMe
CH3
NiBr
Br
NiBi
NiBiSulf
SO3H
COOH
Toluene
Chloroform
Methanol
ε [10^4 M^-1cm^-1]
Fluorescence Intensity norm.
Wavelength [nm]
Wavelength [nm]

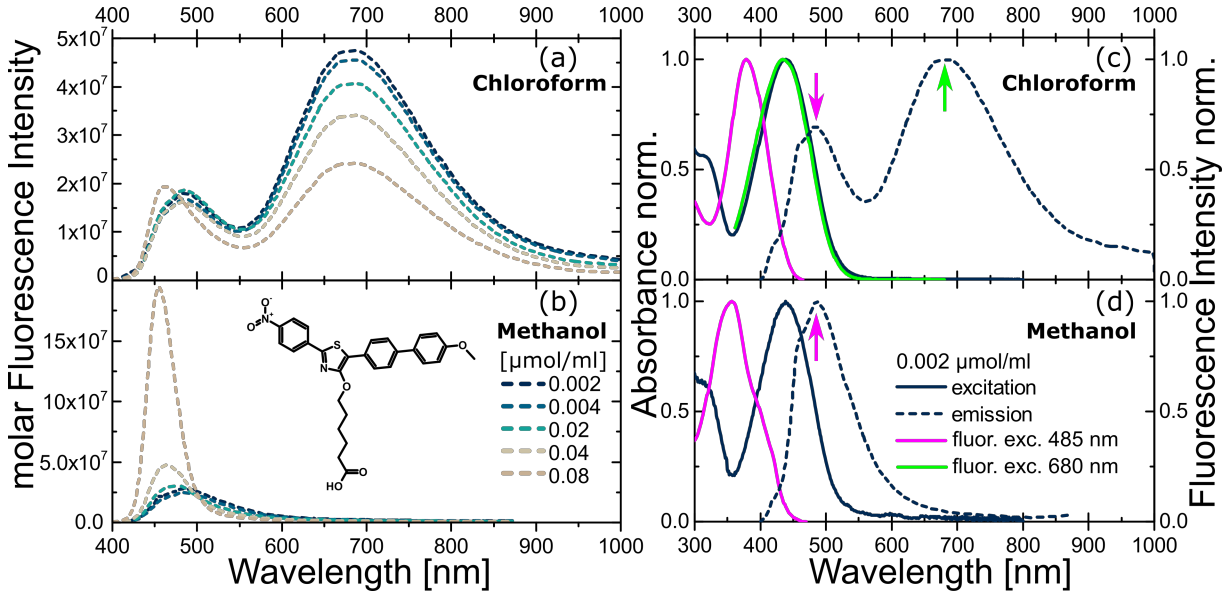
(a)
Chloroform
(b)
Methanol
[µmol/ml]
0.002
0.004
0.02
0.04
0.08
molar Fluorescence Intensity
Wavelength [nm]
(c)
Chloroform
(d)
Methanol
0.002 µmol/ml
excitation
emission
fluor. exc. 485 nm
fluor. exc. 680 nm
Absorbance norm.
Fluorescence Intensity norm.
Wavelength [nm]

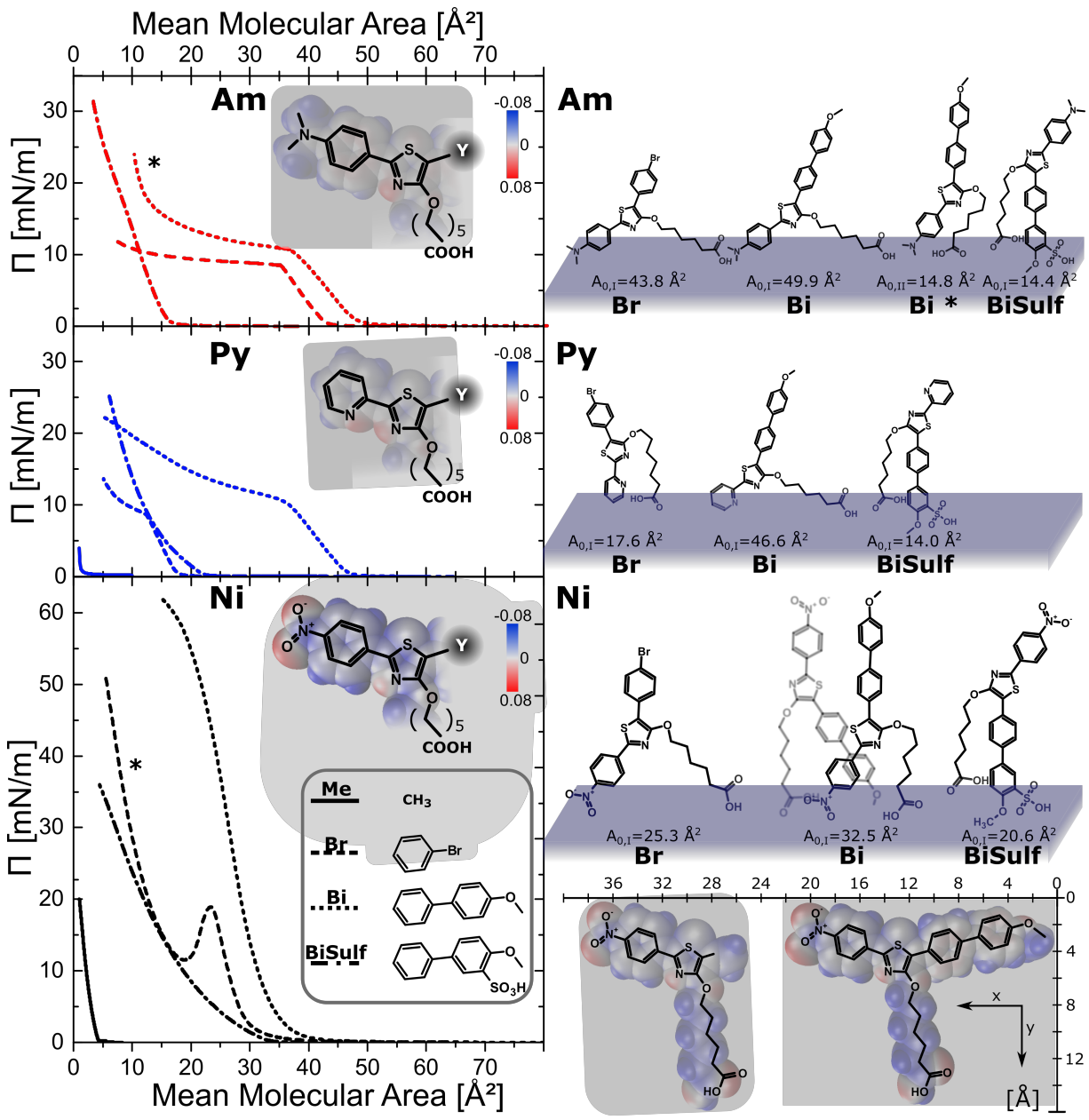
Mean Molecular Area [Å²]
Π [mN/m]
Am
Py
Ni
COOH
Me
CH3
Br
Bi
BiSulf
SO3H
A0,I=43.8 Å²
A0,I=49.9 Å²
A0,II=14.8 Å²
A0,I=14.4 Å²
A0,I=17.6 Å²
A0,I=46.6 Å²
A0,I=14.0 Å²
A0,I=25.3 Å²
A0,I=32.5 Å²
A0,I=20.6 Å²
[Å]

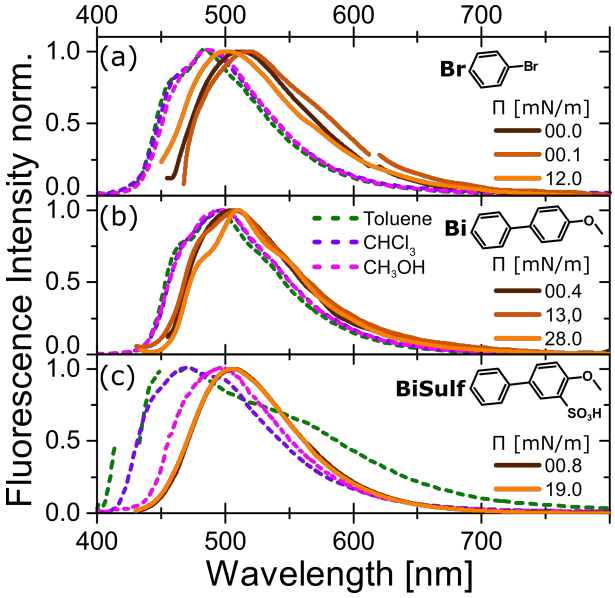
(a)
Br
Br
Π [mN/m]
00.0
00.1
12.0
(b)
Toluene
CHCl3
CH3OH
Bi
O
Π [mN/m]
00.4
13,0
28.0
(c)
BiSulf
O
SO3H
Π [mN/m]
00.8
19.0
Fluorescence Intensity norm.
Wavelength [nm]
0.0
0.5
1.0
400
500
600
700

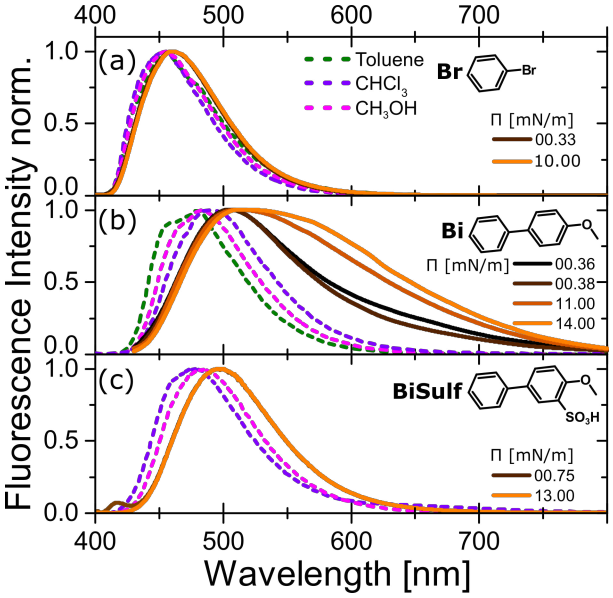
(a)
Toluene
CHCl3
CH3OH
Br
Br
Π [mN/m]
00.33
10.00
(b)
Bi
Π [mN/m]
00.36
00.38
11.00
14.00
(c)
BiSulf
SO3H
Π [mN/m]
00.75
13.00
Fluorescence Intensity norm.
Wavelength [nm]
400
500
600
700
0.0
0.5
1.0

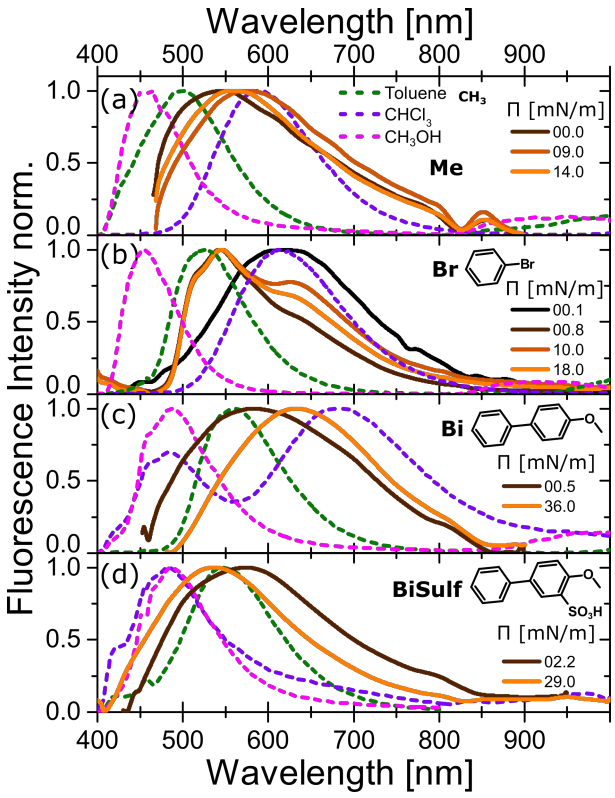
Wavelength [nm]
400
500
600
700
800
900
Fluorescence Intensity norm.
1.0
0.5
0.0
(a)
Toluene
CHCl3
CH3OH
CH3
Me
Π [mN/m]
00.0
09.0
14.0
(b)
Br
Br
Π [mN/m]
00.1
00.8
10.0
18.0
(c)
Bi
O
Π [mN/m]
00.5
36.0
(d)
BiSulf
O
SO3H
Π [mN/m]
02.2
29.0